JOURNAL OF GEOPHYSICAL RESEARCH, VOL. 91, NO. B10, PAGES 10,229–10,245, SEPTEMBER 10, 1986

# Dynamics of Sediment Subduction, Melange Formation, and Prism Accretion

RONALD L. SHREVE

*Department of Earth and Space Sciences and Institute of Geophysics and Planetary Physics*
*University of California, Los Angeles*

MARK CLOOS

*Department of Geological Sciences and Institute for Geophysics, University of Texas, Austin*

The descending plate and overriding block in a subduction zone are analogous to the guide surface and slide block in a slipper bearing, and subducted sediment is analogous to the lubricant. Subduction is more complex and varied, however, because the overriding block is not rigid, the sediment is buoyant, underplating can occur, and sediment supply can vary widely. A model based on the bearing analogy but taking these differences into account makes detailed quantitative predictions for actual sites, which are illustrated by calculations for five diverse examples: Mariana, 16°N; Mexico, 17°N; Lesser Antilles, 13°N (Barbados); Alaska, 153°W (Kodiak); and Japan, 40°N. It requires as input the geometry of the overriding block and the top of the descending plate, the distribution of density and permeability of the overriding block, the speed of subduction, the density and rheological properties of the subducted sediment, and the rate of sediment input. Its predictions include the profile of thickness of the layer of subducted sediment (all sites; maximum of 360 m at Mariana, 5300 m at Japan), the velocities of flow in the layer (all sites), the shear stresses exerted on the walls (all sites; low beneath accretionary prisms, up to 6 MPa beneath Japan), the rate of offscraping (none at Mariana and late Tertiary Mexico; 85% of input at Lesser Antilles; includes melange at Japan), the distribution and rates of underplating (none at Mariana, extensive at Japan), the zones of possible subduction erosion (extensive at Mariana; local at the others), the amount of sediment subducted to the volcanic arc (all sites; 2% of input at Lesser Antilles, 100% at Mariana), the qualitative pattern of flow at the inlet (five basic patterns; all sites), the upward flow of melange in many instances (none at Mariana; extensive at Japan), and, under relatively rare conditions, the formation of large-scale melange diapirs (only at Lesser Antilles beneath Barbados Island).

## INTRODUCTION

The descending plate and overriding block in a subduction zone are analogous to the guide surface and slide block in a slipper bearing. In submarine subduction zones, which on earth are by far the commonest type, the descending plate normally carries a mantle of readily deformed unconsolidated sediment, which it drags downward into a relatively thin subduction channel beneath the overriding block, just as the guide surface drags grease or oil into a thin lubricating layer beneath the slide block (for considerably different applications of this idea, see *Jischke* [1975], *Sorokhtin and Lobkovskiy* [1976], and *England and Holland* [1979]). Subduction zones differ from slipper bearings in certain important respects, however, that make possible much more complex and varied behavior: the overriding block is not rigid but can deform slowly, the buoyancy of the sediment affects the flow, the sediment can underplate onto the hanging wall, and the sediment supply can vary widely relative to the capacity of the system.

This paper presents a mathematical model of the dynamics of sediment subduction, melange formation, and prism accretion based on the bearing analogy. The model applies with no special adjustments to almost all Benioff-type [*Bally*, 1981, p. 14] terrestrial subduction zones. It supplies a logical basis for classification of subduction complexes. And it makes detailed quantitative predictions bearing on a wide variety of geological and geophysical observations. In particular, it predicts (1) the profile of thickness of the subduction channel; (2) the pattern and speeds of flow in the channel; (3) the stresses exerted on the channel walls, which significantly influence the distribution and sizes of nearby earthquakes and the deformation and shape of the overriding block; (4) the amount of sediment offscraped onto the toe of the accretionary prism; (5) the distribution and amount of sediment underplated onto the bottom of the overriding block; (6) the zones of possible subduction erosion of the overriding block; (7) the amount of sediment subducted to the volcanic arc; (8) the qualitative pattern of flow near the inlet to the channel; (9) the upward flow of part of the subducted sediment along the roof of the channel in many instances, a process that *Cloos* [1982] postulated to explain otherwise puzzling petrologic and structural characteristics of parts of the Franciscan subduction complex of California; and (10) the localized extensive accumulation of subduction melange under certain relatively rare conditions, which in turn can give rise to large-scale upwelling and intrusion of melange diapirs.

This model does not address the same questions as the models of *Karig* [1974], *Cowan and Silling* [1978], *Emerman and Turcotte* [1983], *Pavlis and Bruhn* [1983], *Stockmal* [1983], *Davis et al.* [1983], *Dahlen et al.* [1984], *Dahlen* [1984], and *Tharp* [1985]. Whereas those models focus on the deformation of the incoming sediment after incorporation into the accretionary prism, this one focuses on its flow before incorporation into the prism (or subduction to the volcanic arc). Thus it complements the others (and, in fact, can provide some of the boundary conditions they require).

This paper first explicates the assumptions of the model and derives the equations of flow in the subduction channel. Then



Paper number 5B5660.
0148-0227/86/005B-5660$05.00

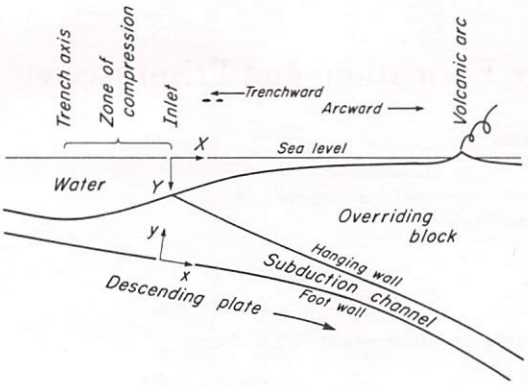


Fig. 1. Geometry of the model, shown schematically. The thickness of the subduction channel is greatly exaggerated in comparison with the thickness of the overriding block. Two coordinate systems are used: $(X, Y)$ to describe the geometry of the overriding block and the top of descending plate, and $(x, y)$ to describe the profile of the subduction channel and flow within it. The accretionary prism, if present, is part of the overriding block, not the zone of compression or the subduction channel.

it discusses the solutions to the equations for both transient state and steady state subduction, explains the method of computation for the steady state case, and outlines the five possible patterns of flow near the inlet, which strongly influence the resulting structure of the upper part of the accretionary prism. Finally, it presents detailed calculations for five widely different representative sites: Mariana, 16°N; Mexico, 17°N; Lesser Antilles, 13°N (Barbados); Alaska, 153°W (Kodiak); and Japan, 40°N.

The geological and geophysical assumptions and implications of the subduction channel model are discussed in more detail in a two-part nonmathematical paper to be published separately (M. Cloos and R. L. Shreve, unpublished manuscript, 1986).

## ASSUMPTIONS AND EQUATIONS

### *Assumptions of Model*

The general geometry of the model is shown in Figure 1. Sediment arrives at the trench axis by conveyance on the descending plate and by deposition from turbidity currents and other (normally minor) sources. As it approaches the inlet of the subduction channel, it undergoes strong longitudinal compression and concomitant thickening, dominantly by imbricate overthrusting to trenchward [*Westbrook and Smith*, 1983, p. 280; *Aoki et al.*, 1983]. It is this zone of compression that is most commonly imaged in seismic reflection studies of convergent plate margins (M. Cloos and R. L. Shreve, unpublished manuscripts, 1986.) At the inlet some or all of the sediment enters the channel, and any excess dewaters and is offscraped [see *Bray and Karig*, 1985]. Within the channel, sediment near the roof is underplated in response to water loss into the hanging wall, except where the shear stress exceeds a critical value. The essential difference between offscraped and underplated material is therefore whether at consolidation and accretion it dewatered directly to the surface or through the overriding block. Some sediment is subducted to the volcanic arc in all cases, because downward shearing will always dominate if the channel becomes thin enough (see also *Batchelor* [1967, p. 226]).

The overriding block is considered to be lithified and hence to deform much more slowly under given stress than the subducted sediment. Thus motion within the block, though doubtless present, is neglected in comparison with motion within the sediment.

An accretionary prism, if present, is here considered part of the overriding block by definition. The zone of compression is not considered part of the prism, contrary to the usage of many investigators, because some, and in certain cases all, of the sediment comprising it is never accreted to the prism but is instead subducted to the volcanic arc. Where offscraping is important, the upper part of the zone grades into the prism, and the boundary between the two is somewhat arbitrary (see forthcoming papers by M. Cloos and R. L. Shreve (unpublished manuscripts, 1986) for more discussion). As will be seen, however, this presents no serious difficulties.

Positions in the model are specified in terms of two coordinate systems (Figure 1): an orthogonal curvilinear system $(x, y)$ in the subduction channel, in which $x$ is measured from the inlet along the curved foot wall, and a cartesian one $(X, Y)$ elsewhere, with origin at sea level directly above the inlet. Note that $Y$ is positive downward.

The profile of the foot wall is considered given. The descending plate moves beneath the overriding block at given uniform speed $U$. The distribution of density and permeability of the overriding block, which is assumed water-saturated, are considered given; and the density of the water $\rho_w (= 1.0$ Mg $m^{-3})$ is assumed uniform.

The thickness of the channel, which includes only the flowing sediment and not the accretionary prism, is described by the profile $y = h(x)$, whose calculation is a principal objective. The thickness $h$ is assumed small in comparison with the thickness of the overriding block and only slowly varying in the $x$ direction. In other words, $h' \ll 1$, where the prime here and elsewhere denotes differentiation with respect to $x$. This means that the hanging wall and the foot wall are assumed relatively smooth at a scale comparable to the channel thickness. Thus this assumption fails within a few channel thicknesses of subducting seamounts (which normally are only local and temporary perturbations). It also fails near horsts and grabens in the top in the downgoing plate (which probably are important only near relatively sharp bends in the foot wall).

The principal variables governing the flow in the channel are the pressure exerted by the hanging wall on the flowing sediment, the buoyancy of the relatively low density sediment, and the shearing between the walls.

The pressure, denoted by $p_H$, is to good approximation the lithostatic pressure due to the weight of the overlying rock, inasmuch as the shear stresses in the sediment will be negligible in comparison with the normal stresses except very near the inlet [*Batchelor*, 1967, p. 221] and the tectonic stresses in the crust will be small in comparison with the lithostatic pressure except very near the surface. Thus the densities of the overlying rocks are an important element of the model.

The buoyancy is governed by the density of the sediment. The sediment in the subduction channel is water saturated and only weakly consolidated. The only way its density can increase significantly is through loss of pore water to the hanging wall, inasmuch as its temperature is so low that recrystallization is unimportant. The resultant dewatering not only increases the density but also significantly increases the viscosity of the sediment next to the hanging wall, which causes underplating (see forthcoming papers by M. Cloos and R. L. Shreve (unpublished manuscripts, 1986) for more dis-

cussion). The density and viscosity of the rest of the sediment in the channel therefore remain practically unaffected inasmuch as the dewatered sediment is removed from the channel as soon as it forms. Hence the density $\rho_s$ of the subducting sediment is to good approximation the same everywhere along the channel. In particular, it does not increase with depth, as intuition might suggest. It is somewhat greater than $\rho_A$, the density of the trench fill, because of weak consolidation by water loss directly to the surface in the zone of compression. Likewise, the viscosity of the subducting sediment is approximately uniform and independent of depth.

In the great majority of cases, examples being Japan, 40°N, and Alaska, 153°W, in which the trench sediments move toward the inlet relatively quickly, $\rho_A$ is typically near 2.0 Mg $m^{-3}$, and $\rho_s$ is probably about 2.2 Mg $m^{-3}$ (this is discussed further by M. Cloos and R. L. Shreve (unpublished manuscript, 1986)). These are therefore the values used throughout this paper, unless otherwise specified. In exceptional cases, such as the Lesser Antilles, 13°N, however, the sediments move toward the inlet so slowly that they have time to dewater to somewhat higher than normal densities. In these cases, the values of $\rho_A$ or $\rho_s$ or both must be adjusted appropriately.

The shearing in the subduction channel is governed by the speed $U$ of the foot wall and the viscosity $\mu_s$ of the sediment. Although all evidence suggests that the viscosity is strongly dependent on strain rate, it is taken to be independent of it (that is, to be Newtonian), both because the appropriate flow law is unknown and because the essential physics will be no different, although of course the details will differ quantitatively (M. Cloos and R. L. Shreve, unpublished manuscript, 1986). The value used, except where otherwise specified (namely, $7 \times 10^{17}$ Pa s, or $7 \times 10^{18}$ poise), is comparable to values estimated by *England and Holland* [1979, p. 290], *Emerman and Turcotte* [1983, p. 383], and *Jackson and Talbot* [1986] and accords with independent estimates for weak rocks at comparable strain rates [*Kehle*, 1970, p. 1660; *Carter*, 1976]. In addition, it agrees with the limitations on settling rate necessary to enable "exotic" blocks in melange to be carried to shallow depths [*Cloos*, 1982, p. 338] and gives reasonable results.

The rate of underplating is governed by the rate at which water can escape into the hanging wall. An exception to this rule must be made, however, in order to account for the anomalous lack of underplating in places, such as Mariana, 18°N, where the viscous drag on the hanging wall, and hence the shear stress and strain rate in the adjacent sediment, is high. Hence underplating is assumed to occur only where the drag is less than a certain critical value $D_{HC}$. In reality, of course, the cutoff would no doubt be more gradual. Inasmuch as no relevant experimental data are available, the value adopted (namely, 1.5 MPa, or 15 bars), can be justified only on the basis that it has plausible magnitude and gives reasonable results.

If $V_H$ is the component of velocity of the imminently underplated sediment toward the hanging wall, $V_U$ is the thickness of new rock added to the hanging wall in unit time, and $q_w$ is the volume rate of water loss into the hanging wall, conservation of both water and solids requires that

$$V_H = q_w\left(\frac{\rho_U - \rho_w}{\rho_U - \rho_s}\right) \qquad V_U = q_w\left(\frac{\rho_s - \rho_w}{\rho_U - \rho_s}\right) \tag{1}$$

where $\rho_U$ (= 2.4 Mg $m^{-3}$ typically) is the density of the newly underplated rock. Although hydration of some of the wall rocks, as for example in serpentinization of peridotites, may initially use some, or even most, of the lost water, eventually the bulk of it will percolate toward the surface, driven by the essentially lithostatic pore pressure in the subduction channel. Thus the rate of underplating is governed primarily by the pressure $p_H$ in the subduction channel and the permeability of the overlying block.

Unfortunately, the permeabilities of rocks in place are extremely diverse, with measured values ranging over more than 9 orders of magnitude [*Brace*, 1980, p. 244]. In general, however, the near-surface values for fine-grained sedimentary rocks such as typify trench fills and therefore accretionary prisms [*von Huene*, p. 1984, p. 367] are of the order of $10^{-18}$ $m^2$ (1 microdarcy) or less, whereas those for crystalline ones are of the order of $10^{-15}$ $m^2$ (1 millidarcy). This difference reflects the differing origin of the permeability in the two cases: mainly interconnected pores in the sedimentary rocks (except where hydraulic fracturing is important) and cracks in the crystalline ones. Hence the two cases must be considered separately.

According to measurements by *Bryant et al.* [1975, p. 13] the permeabilities of both consolidated and unconsolidated mud-rich sediments from the Gulf of Mexico are well approximated by the empirical relationship

$$k_{sr} = A \exp B$$

where $\rho_{sr}$ is the bulk density of the sediments, $A = 2.75 \times 10^{-10}$ $m^2$, and $B = 9.45$ $Mg^{-1}$ $m^3$. This relationship also fits data from several trench axis and trench slope environments (W. R. Bryant, personal communication, 1984). The permeabilities of the somewhat more sandy sediments of many other trench axis environments should be somewhat greater. The permeability given by the formula was therefore used for the entire accretionary prism and other sedimentary rocks (hence the subscripts *sr*) at sites where they are likely to be more mud-rich. Where they are likely to be more sand-rich, on the other hand, as at Mexico, 17°N, which receives sediment from a nearby submarine canyon, 3 times the formula value was used.

These estimates disregard possible additional permeability due to hydraulic fracturing, which many workers believe may be dominant in accretionary prisms. Our conclusion is that on the contrary, hydraulic fracturing does not significantly affect the large-scale permeability of accretionary prisms, although it is likely to occur near the surface in many of them (see forthcoming papers by M. Cloos and R. L. Shreve (unpublished manuscripts, 1986) for full discussion).

The permeabilities of crystalline rocks must drop off considerably at depth, inasmuch as both the subsidence of certain forearc basins overlying crystalline basement and the presence of "exotic" blueschist blocks in some melanges imply a very small or zero rate of underplating, and hence of water loss, at depths of 20 to 30 km. The available measurements [*Brace*, 1980] evidence no strong trend, but they extend only to about 3 km. Hence no rigorous basis for predicting the form or magnitude of the drop-off exists, making it necessary to assume a simple reasonable form, such as an exponential decrease, with parameters adjusted to satisfy known constraints.

The permeability $k_{cr}$ of the crystalline rocks (hence the subscripts *cr*) at depth $Y$ is therefore assumed to be given by

$$k_{cr} = k_0 \exp -\lambda_{cr} Y \tag{2a}$$

where $k_0$ is the sea level permeability and $\lambda_{cr}$ is a constant to

be adjusted. Integrating Darcy's law from the surface to the hanging wall at depth $Y_H$ and eliminating $q_w$ by means of (1) then gives

$$V_U\left(\frac{\rho_U - \rho_s}{\rho_s - \rho_w}\right) = \frac{k_0\lambda_{cr}(p_H - \rho_w g Y_H)}{\mu_w(\exp \lambda_{cr} Y_H - 1)} \tag{2b}$$

in which $g$ ($=9.8$ m s$^{-2}$) is the acceleration due to gravity. The derivation assumes that hydration reactions, such as serpentinization, are negligible, as at Mexico, 17°N, where underplating apparently is small or absent beneath the granite basement, so that upward water flow $q_w$ is approximately the same at all depths. The viscosity of water $\mu_w$ ($=1$ mPa s), which varies little with pressure but significantly with temperature, is taken to be uniform because of the low geothermal gradient above the relatively cold descending plate. Finally, taking, say, 5 to 10 m Ma$^{-1}$ for $V_U$, 20 to 30 km for $Y_H$, 2.7 to 3.4 Mg m$^{-3}$ for the density of the overlying rock, and $10^{-15}$ m$^2$ (1 millidarcy) for $k_0$ gives a value for $\lambda_{cr}$ of approximately 0.7 km$^{-1}$.

With these results the potential rate of underplating at all points of the hanging wall can readily be found by means of a more messy version of (2b) that takes into account the layers of sedimentary and crystalline rock in the overriding block and of any overlying layers of still consolidating sediment (defined as any with density of less than 2.4 Mg m$^{-3}$), in which the pressure gradient is lithostatic.

*Equations of Sediment Subduction*

It is more convenient to work with the hydraulic potential

$$\Phi = p_H - \rho_w g Y_I - \rho_s g(Y - Y_I) \tag{3}$$

than with the pressure $p_H$, where $Y_I$ is the depth of water at the inlet, because $\Phi$ combines the effects of buoyancy and pressure. Because $h' \ll 1$, the potential varies negligibly in the $y$ direction; hence it is to good approximation a function only of $x$ [*Batchelor*, 1967, pp. 179, 218]. Under the assumptions of the model the potential $\Phi$ and its derivative $\Phi'$ are known functions calculated from the structure of the overriding block.

To first order in the small quantity $h'$ the $x$ component of velocity of the subducting sediment is governed by the basic differential equation of hydrodynamic lubrication theory

$$\frac{d^2u}{dy^2} = \frac{\Phi'}{\mu_s} \tag{4a}$$

with boundary conditions $u(0) = U$, $u(h) = 0$. Thus solving,

$$u = \frac{U}{h}(h - y) - \frac{\Phi'}{2\mu_s} y(h - y) \tag{4b}$$

[*Batchelor*, 1967, pp. 182, 220]. The viscous drag (that is, shear stress) on the hanging wall, defined as positive in the arcward direction, is given by

$$D_H = -\mu_s \left.\frac{\partial u}{\partial y}\right|_{y=h} = \frac{\mu_s U}{h} - \tfrac{1}{2}\Phi' h \tag{5a}$$

and that on the foot wall, defined as positive in the trenchward direction, by

$$D_F = -\mu_s \left.\frac{\partial u}{\partial y}\right|_{y=0} = \frac{\mu_s U}{h} + \tfrac{1}{2}\Phi' h \tag{5b}$$

Integrating (4b) with respect to $y$ from foot wall to hanging wall then gives the net volume discharge of sediment $Q$ as a function of $h$,

$$Q = \tfrac{1}{2}Uh - \frac{\Phi' h^3}{12\mu_s} \tag{6a}$$

Conservation of mass requires that $Q$ and $h$ also satisfy the continuity equation

$$\begin{aligned} \frac{\partial Q}{\partial x} + \frac{\partial h}{\partial t} &= -V_H \qquad |D_H| < D_{HC} \\ \frac{\partial Q}{\partial x} + \frac{\partial h}{\partial t} &= 0 \qquad \text{otherwise} \end{aligned} \tag{6b}$$

in which $t$ denotes time, and the potential rate of sediment loss $V_H$ is a known function of $x$.

Equation (6a) says that where $\Phi'$ is positive, $Q$ cannot exceed a certain value, the local capacity $C_L$, given by

$$C_L = \left(\frac{2\mu_s U^3}{9\Phi'}\right)^{1/2} \tag{7a}$$

which is the maximum of $Q$ (for positive $h$) found by setting the derivative of the right-hand side of (6a) to zero. Where $\Phi'$ is zero or negative, on the other hand, the local capacity is unlimited. The maximum rate at which sediment can enter the subduction channel in a steady state, termed the global capacity $C_G$, is controlled by that point in the channel where the local capacity plus the cumulative upstream loss to underplating is least; that is,

$$C_G = \min\left[C_L(x) + \int_0^x V_H\, dx\right] \tag{7b}$$

A minimum in local capacity that limits the amount of sediment that actually passes it is termed a control point (otherwise, it is merely a potential control point).

If $\Phi'$ is zero or negative throughout the channel, the global capacity is unlimited, and the rate at which sediment enters the channel is then simply its availability at the trench axis, namely,

$$Q_A = \rho_A U h_A / \rho_s \tag{7c}$$

where $h_A$ is the depth of sediment at the axis adjusted to include the small additional influx between the axis and inlet.

Because of loss to underplating the sediment discharge progressively diminishes arcward. It can never reach zero, however, because for sufficiently diminished discharge the drag on the hanging wall will exceed the critical value $D_{HC}$, which will prevent underplating and hence further loss.

Although the equations can be treated as is, it is more convenient to transform to the dimensionless variables

$$\begin{gathered} \xi = Ux/3Q_* \qquad \zeta = y/h \qquad \tau = U^2 t/9Q_* \\ \varphi = u/U \qquad \kappa = Uh/3Q_* \qquad \Upsilon = Q/Q_* \\ \delta_H = D_H h/\mu_s U \qquad \delta_{HC} = D_{HC} h/\mu_s U \qquad \delta_F = D_F h/\mu_s U \end{gathered} \tag{8a}$$

and the dimensionless flow and loss parameters

$$\alpha = \frac{9Q_*{}^2\Phi'}{2\mu_s U^3} \qquad \beta = \frac{3V_H}{U} \tag{8b}$$

in which the representative discharge $Q_*$ is either $C_s$ or $Q_A$ as appropriate. Equations (4b), (5), and (6) then take the forms

$$\varphi = (1 - \zeta)(1 - \alpha\kappa^2\zeta) \tag{9}$$

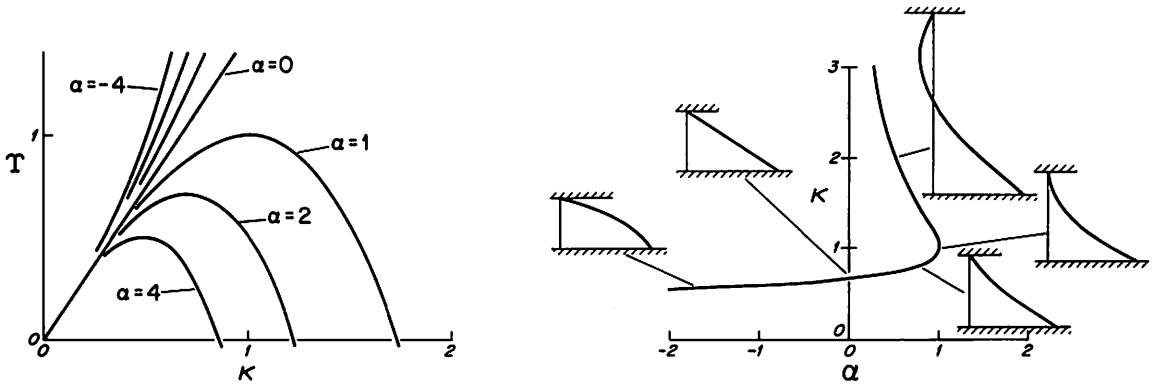


Fig. 2. (Left) Dimensionless net sediment discharge $\Upsilon$ versus dimensionless subduction channel thickness $\kappa$ for various values of the dimensionless flow parameter $\alpha$. Curves for $\alpha$ positive resemble the flow-concentration curves for the kinematic wave theory of traffic flow [*Lighthill and Whitham*, 1955*b*], whereas those for $\alpha$ negative resemble the curves for flood movement [*Lighthill and Whitham*, 1955*a*]; the subduction channel therefore behaves correspondingly. (Right) Thickness $\kappa$ versus parameter $\alpha$ for unit discharge $\Upsilon$, showing representative velocity profiles.

$$\delta_H = 1 - \alpha\kappa^2 \qquad \delta_F = 1 + \alpha\kappa^2 \tag{10}$$

$$\Upsilon = \tfrac{1}{2}\kappa(3 - \alpha\kappa^2) \tag{11a}$$

$$\frac{\partial\Upsilon}{\partial\zeta} + \frac{\partial\kappa}{\partial\tau} = -\beta \qquad |\delta_H| < \delta_{HC}$$

$$\frac{\partial\Upsilon}{\partial\zeta} + \frac{\partial\kappa}{\partial\tau} = 0 \qquad \text{otherwise} \tag{11b}$$

The parameters $\alpha$ and $\beta$ are known functions of $\xi$ computed from the given characteristics of the overlying block. The key relationship (equation (11*a*)) and representative velocity profiles (equation (9)) are plotted in Figure 2.

## Solution of Equations

### *Transient State Subduction*

Equations (11) are kinematic wave equations [*Lighthill and Whitham*, 1955*a*, pp. 281–285, 310]. The kinematic wave speed is given by

$$c = \tfrac{1}{3}U\frac{\partial\Upsilon}{\partial\kappa} = U\left(\frac{\Upsilon}{\kappa} - 1\right) = 3\bar{U} - U \tag{12}$$

where $\bar{U} = Q/h$ is the mean speed of flow. It is zero where sediment discharge equals the local capacity and ranges from $3\bar{U}$ for $\Phi'$ large and negative to $\frac{1}{2}U$ for $\Phi'$ equal to zero to $-3\bar{U}$ for $\Phi'$ large and positive.

Three cases have to be distinguished, according as $\Phi'$, or equivalently $\alpha$, is everywhere positive, everywhere negative, or mixed.

Case 1, $\alpha$ everywhere positive, encompasses almost all actual situations, because in order for $\Phi'$ to be negative at some point the pressure, which normally increases arcward, instead must decrease steeply enough to offset the buoyancy. For $\alpha$ positive the curves of discharge versus thickness (Figure 2, left) closely resemble the flow-concentration curves for traffic flow [*Lighthill and Whitham*, 1955*b*]; hence the resultant behavior will be qualitatively similar.

Thus if sediment is supplied to the trench axis at a steady rate less than the global capacity, all of it is subducted, $\kappa$ has the smaller of the two positive values possible for given $\Upsilon$ (Figure 2), and no flow reversal occurs [*Lighthill and Whitham*, 1955*b*, pp. 331–332]. The accretionary prism can grow only by underplating of material onto the hanging wall and deposition of new sediment on the trench slope. Variations in the rate of sediment supply propagate down the channel, and because $c$ decreases with $Q$, variations in channel thickness accompanying drops in supply steepen as they propagate [*Lighthill and Whitham*, 1955*b*, pp. 327–331]. As the resulting abrupt jumps pass by, the hanging wall is sharply bent and then unbent. The two strains are essentially equal and opposite. Thus if earthquakes are generated, some of them should produce first motions opposite those due to the general shearing between the two plates, and so they would be anomalous events. They are likely to be small, however, because of the small volumes that are strained.

If the sediment supply is gradually increased to a new steady rate greater than the global capacity, only part of it is subducted, $\kappa$ shifts to the larger of its two possible positive values (Figure 2), and flow reversal occurs [*Lighthill and Whitham*, 1955*b*, p. 332]. The shift in channel thickness $\kappa$ takes place as an abrupt jump (a shock) that originates at the control point and propagates trenchward (Figure 3) with a speed that is greater the smaller the jump and the more the sediment supply exceeds capacity [*Lighthill and Whitham*, 1955*b*, p. 332–334]. The jump appears at the upper surface of the overriding block as a wave of uplift migrating trenchward. It is likely to be hundreds or even thousands of meters high, as will be seen, so that the resulting earthquakes, if any, could be relatively large. Moreover, some would have anomalous first motions. They are not likely to be common, however, because they can occur only while a subduction channel is adjusting to a change in sediment supply from less to greater than capacity, which is an infrequent and slow process.

After adjustment is complete, sediment discharge at any point equals the global capacity less the trenchward loss to underplating, and fluctuations in sediment supply have no effect on the subduction channel unless they drop below the global capacity. The subduction channel in the zone of reverse flow contains three layers: near the foot wall, downgoing sediment that passes the control point; in the middle, downgoing sediment that before reaching the control point turns back to supply the reverse flow; and near the hanging wall, upgoing sediment that farther trenchward variously may underplate onto the hanging wall, emerge at the inlet, or rejoin the middle layer, forming a whirlpoollike gyre. The upgoing sediment is

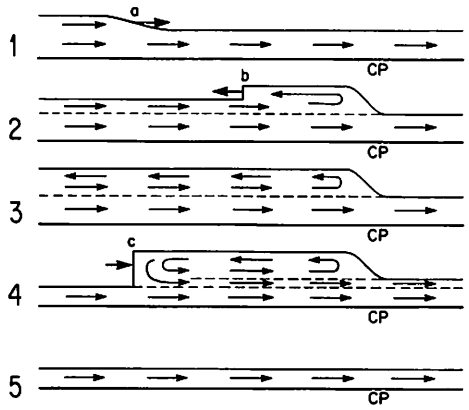


Fig. 3. Transition to reverse flow and back, shown schematically in five stages: (1) After channel reaches steady state with sediment input just equal to global capacity, input increases, causing a wave (labeled "a") of higher discharge and greater channel thickness to propagate arcward. (2) When the wave reaches the control point (labeled "CP"), a region of reverse flow forms there and expands trenchward behind an abrupt jump (labeled "b"). (3) Reverse flow continues unchanged as long as input remains above capacity. (4) If input decreases to below capacity, a zone of no reverse flow reforms at the inlet and expands arcward behind the abrupt jump (labeled "c"). (5) Finally, flow everywhere is less than capacity.

intensely deformed when it turns back and may contain metamorphic minerals or "exotic" blocks from higher-pressure environments; hence it is here termed subduction melange (so called to differentiate it from melange formed by other processes, such as submarine sliding). The accretionary prism can grow not only by underplating of material onto the hanging wall and deposition of new sediment on the trench slope but also by offscraping of subduction melange or excess sediment or both at the inlet. The fact that the lowermost layers of sediment carried on the downgoing plate are least likely to be offscraped or turned back by reverse flow explains the relative scarcity of rocks derived from basal pelagic sediments, such as oozes, cherts, and metalliferous layers, in accretionary complexes [*Moore*, 1975].

In case 2, $\alpha$ everywhere negative, the curves of discharge versus thickness (Figure 2, left) resemble the flow-concentration curves for flood movement [*Lighthill and Whitham*, 1955*a*]. All sediment supplied to the trench axis is subducted, $\kappa$ has only one possible value (Figure 2), and no flow reversal occurs. The accretionary prism grows by underplating and deposition but not offscraping. Variations in the rate of sediment supply propagate down the subduction channel, as in case 1, but because kinematic wave speed $c$ increases with sediment discharge $Q$, it is variations in channel thickness due to rises in supply that progressively steepen into abrupt jumps [*Lighthill and Whitham*, 1955*a*]. As before, the resulting earthquakes, if any, are likely to be small.

In case 3, $\alpha$ mixed, many variants are possible, but all behave according to the same principles as the simplest and most likely possibility, namely, $\Phi'$ (and hence $\alpha$) negative over a short reach somewhere in the channel and positive above and below. The part above behaves exactly as in case 1, whereas the part below behaves differently according to whether its capacity is greater or less than that of the upper part. If greater, the sediment delivered to it simply behaves as in case 1 with sediment supply less than capacity. If less, on the other hand, not all of the sediment delivered to it can pass through, flow reversal occurs as in case 1 with sediment supply greater than capacity, and subduction melange accumulates just below the negative reach just as it does at the inlet when excess sediment is supplied. In this case, however, sufficient accumulation of the relatively low density melange can result in convective instability and hence upward intrusion of a melange diapir. In some cases, "xenoliths" of previously underplated wall rock may be detached and incorporated into the rising melange.

### *Steady State Subduction*

No matter how long sediment is supplied at a constant rate, a subduction channel can never reach a truly steady state if the accretionary prism grows. Like the deformation of the prism, however, this growth is so slow in comparison with the transient processes in the channel that a quasi-steady condition is attained which can be idealized as steady with little loss in accuracy and great gain in simplicity.

For a steady state the time derivative in (11*b*) is zero. Integration of the resulting ordinary differential equation gives for the dimensionless discharge

$$\Upsilon = \Upsilon_I - \int_0^{\xi} \psi \, d\xi \tag{13}$$

in which $\Upsilon_I = \Upsilon(0)$ and $\psi$ is $-\beta$ for $|\delta_H| < \delta_{HC}$ and zero otherwise. With $\Upsilon$ known, the dimensionless channel thickness $\kappa$ can be found from (11*a*), and then the dimensionless velocity profile $\varphi$ and drags $\delta_H$ and $\delta_F$ can be found from (9) and (10). For case 1 with sediment input $Q_A$ less than global capacity $C_G$, $\Upsilon_I = Q_A/C_G$, and $\kappa$ is the smaller positive root of (11*a*) in accordance with the discussion of the transient state. Similarly, for the same case with $Q_A > C_G$, $\Upsilon_I = 1$, and $\kappa$ is the larger positive root. For case 2, $\Upsilon_I = 1$, and $\kappa$ is the only positive root. Finally, for case 3, the alternating reaches of positive and negative $\alpha$ are treated, starting at the inlet, like cases 1 and 2, respectively.

### *Computation of Results*

The model is implemented for steady state subduction as a computer program that finds the channel thickness and other desired quantities at 1-km intervals in the horizontal distance $X$ from the inlet. The input data fall into two categories: (1) parameters that are assumed identical at all sites (except where otherwise specified in special cases) and (2) those that define the characteristics of specific sites. The first category consists of the densities $\rho_s$ and $\rho_A$ and viscosity $\mu_s$ of the sediment, the critical drag $D_{HC}$ for cutoff of underplating, the density $\rho_U$ of newly underplated rock, the constants describing the permeabilities of the overlying rocks, such as $k_0$ and $\lambda_{cr}$ for the crystalline rocks, and the density $\rho_w$ and viscosity $\mu_w$ of water. These parameters have already been discussed along with the other general assumptions of the model. The second category consists of the subduction speed $U$; the sediment depth at the trench axis, $h_A$; the geometry of the descending plate; and the structure, densities, and types (mud-rich sedimentary, sand-rich sedimentary, or crystalline) of the rocks of the overriding block.

The program begins by computing tables of the subduction channel pressure $p_H$, the hydraulic gradient $\Phi'$, and the potential water loss $q_w$ at 1-km intervals in $X$.

It computes $p_H$ as the lithostatic pressure due to the column of rock and water, if any is present, vertically overlying the

point in question. The result therefore sharply mirrors minor features of the surface topography and bedrock structure whose effects in reality are spread over distances comparable to their heights above the point in question. To compensate for this, the input topography and structure are appropriately generalized. The degree of approximation involved is commensurate with that of the model as a whole. Besides, anything even a little more precise would require considerably more detailed information than is currently available on the structure, conditions, and properties of the overlying rocks.

The program computes the derivatives $\Phi'$ as the differences between the values of $\Phi$ at points 1 km in $X$ (horizontally) arcward and trenchward of the point in question, divided by the distance between them along the foot wall. This can cause spurious results in certain relatively rare cases of slight mismatch in the computed $p_H$ below vertical boundaries in the overriding block. Moreover, the diagrammatic geometry used in order to limit computing costs produces sharp step jumps in $\Phi'$, in conflict with the more gradational character of the actual rocks. At all such places, therefore, $\Phi'$ was smoothed according to the cubic spline formulas $\Phi'_{S,0} = \frac{1}{2}(\Phi'_{U,+1} + \Phi'_{U,-1})$ and $\Phi'_{S,\pm 1} = (1/32)(-\Phi'_{U,\mp 2} + 6\Phi'_{U,\mp 1} + 18\Phi'_{U,\pm 1} + 9\Phi'_{u,\pm 2})$, where the subscripts $S$ and $U$ refer to the smoothed and unsmoothed values and 0, $-1$, and $+1$ refer to the points at the place in question and 1 km (horizontally) trenchward and arcward of it. This was the only such smoothing done. It rounds what otherwise would be sharp steps in the output curves.

The program computes the potential water loss $q_w$ as if the lost water percolates vertically upward to the surface. In actuality it deviates toward regions of higher permeability (that is, toward the crystalline rocks at depths of less than about 15 km and away from them at greater depths). Thus the approximation is best where contacts between sedimentary and crystalline rocks either are nearly horizontal or are relatively distant, which is generally the case.

The actual water loss, and hence the underplating rate, depend on the drag $D_H$ on the hanging wall. Normally $|D_H|$ is either much greater or much less than the critical value $D_{HC}$, and the loss is accordingly either zero or the full potential rate. In the relatively rare circumstances in which $|D_H|$ increases in the arcward direction if underplating occurs and decreases if it does not, however, conditions can be such that the drag locks onto the critical value, and the underplating rate takes an intermediate value determined by the condition $|D_H| = D_{HC}$.

A related but improbable theoretical possibility, never observed in the computations, is the opposite situation, in which case the underplating rate is not uniquely determinable. Instead, small random variations at the (trenchward) point where the drag reaches the critical value govern whether it is zero or full.

Once the program has generated the required tables of $\Phi'$ and $q_w$, it computes corresponding tables of the subduction channel thickness, sediment discharge, and other desired quantities. First, working arcward from the inlet, it computes $h$, $Q$, and so on, assuming no reverse flow, finding by trapezoidal integration the loss due to underplating, noting the location of potential control points at places where the arriving sediment discharge exceeds the local capacity, continuing onward from these places with $Q$ set to $C_L$, and stopping when it reaches either the end of the tables (that is, the volcanic arc) or a transition of $\Phi'$ from negative to positive. Then, working trenchward from the previously noted potential control points taken in reverse order, it redoes the computations, this time assuming reverse flow, and stopping either at the inlet or, more commonly, where the reverse flow peters out owing to the greater rate of underplating caused by the lower drag on the hanging wall associated with reverse flow. Finally, if it has not yet reached the end of the tables, it notes the most arcward point reached as a potential site of melange accumulation and diapiric intrusion and, treating this location like the inlet, repeats the whole process.

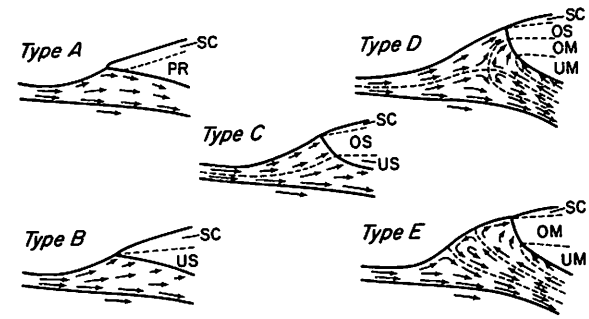


Fig. 4. Qualitative flow patterns near inlet, showing the five possible types. Materials in accretionary prism can be slope cover (SC), preexisting rock (PR), offscraped sediment (OS), underplated sediment (US), offscraped melange (OM), and underplated melange (UM).

*Patterns of Flow at Inlet*

Inasmuch as the equations assume longitudinal compression or extension small in comparison with the wall-parallel shear, they do not apply near the inlet. This raises the possibility that the inlet could actually have smaller capacity than the equations predict. If so, the resultant offscraping would build the leading edge of the prism trenchward, eventually making it less blunt, which in turn would decrease $\Phi'$ and hence increase capacity. The inlet therefore trends to evolve toward a geometry such that the amount of sediment subducted is that which the equations predict. Thus the details of flow at the inlet do not significantly affect the steady state behavior of the subduction channel.

They do, however, strongly influence the structure of the upper part of the accretionary prism, which is the part most accessible to observation. Qualitatively, five patterns of flow, here termed types A through E, are possible (Figure 4). At the trench axis the sediment in every case simply rides along passively without deformation, and in the zone of compression between the axis and the inlet it undergoes longitudinal compression, basal shearing, and surface steepening as the moving foot wall drags it against the fixed leading edge of the hanging wall. The differences between the types lie in their patterns of offscraping and underplating at the inlet.

In type A all of the arriving sediment is subducted. None is offscraped, and because drag on the hanging wall is high, none is underplated at the inlet. The hanging wall in this case would in actuality most likely undergo subduction erosion (a process not incorporated into the present version of the model) and hence long-term subsidence. The structure at shallow depths on the trench slope therefore consists of preexisting rock overlain by directly deposited slope cover sediment, which of course could be modified by such processes as erosion, slumping, folding, and faulting.

In type B all of the arriving sediment is subducted and none

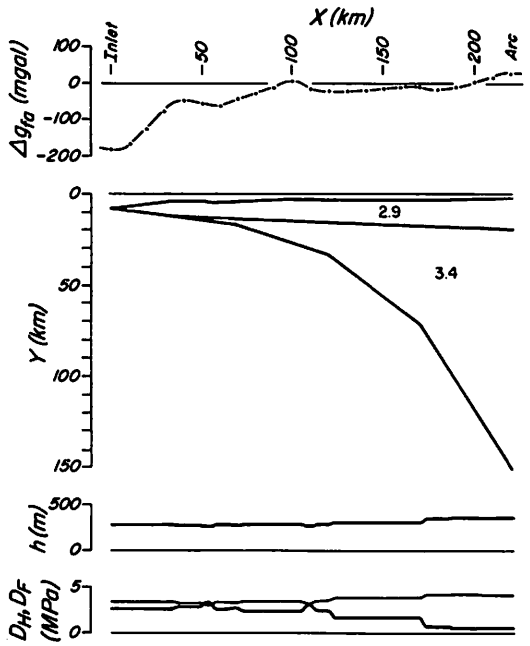


Fig. 5. Mariana, 18°N. $U = 40$ km Ma$^{-1}$ (half of actual present speed, because backarc spreading is disregarded); $h_A = 150$ m (present thickness at site). Density cross section used in calculation, showing densities in megagrams per cubic meter. Rocks are all crystalline. The graph above the density cross section shows the free air gravity anomaly observed (broken heavy curve [*Watts*, 1976]) and calculated (dots; the calculation assumes that the descending plate consists of 7-km-thick crust with density of 2.9 Mg m$^{-3}$ overlying rock with density of 3.4 Mg m$^{-3}$). The upper graph below the cross section shows the thickness of the subduction channel; the lower one shows drags (shear stresses) on the hanging wall (heavy curve) and foot wall (light curve). Subduction erosion, such as *Hussong and Uyeda* [1982, p 920] suggested for this site, is possible (and would be even more likely at the actual present subduction speed of 80 km Ma$^{-1}$).

is offscraped, but some is underplated. In this case the prism grows forward very slowly, because underplating on the inclined hanging wall at the inlet has a small horizontal component toward the trench. Growth by processes analogous to offscraping is also possible (M. Cloos and R. L. Shreve, unpublished manuscript, 1986.) The slope cover overlies underplated sediment (or, high on the slope, possibly preexisting rock) and the slope undergoes long-term uplift. The accretionary prism thickens faster than it grows trenchward, thereby gradually reducing inlet capacity and eventually causing offscraping and thus a change to type C. Hence this type should be relatively rare.

In type C some of the arriving sediment is offscraped, some is underplated, and the rest is subducted. The slope cover is separated from the underplated sediment by an intervening layer of offscraped sediment, and as in type B, the slope undergoes long-term uplift. In addition, the prism grows trenchward faster than it thickens, thereby widening with time (until limited by internal deformation).

In type D some of the arriving sediment is offscraped and the rest is subducted, but reverse flow brings subduction melange to the inlet, where some of it is underplated, some is offscraped beneath the offscraped sediment, and the rest is resubducted. The slope cover overlies offscraped sediment, which in turn overlies melange. Differentiation between the offscraped and the underplated parts of the melange would almost certainly be impossible in practice. The slope in this type undergoes long-term uplift possibly punctuated by transient episodes of more rapid uplift or subsidence due to fluctuations in sediment supply, and as in type C, the prism widens with time.

In type E all of the arriving sediment is subducted, but reverse flow brings subduction melange to the inlet, where some of it is offscraped and the rest is resubducted. In this case the slope cover directly overlies offscraped and underplated melange, the slope undergoes uplift and subsidence as in type D, and the prism widens.

The present calculations can predict types A, B, and C unambiguously. For type C the amount of sediment offscraped is simply the difference between the sediment input $Q_A$ and the local capacity at the inlet as computed from (7*a*). The calculations can also predict type D unambiguously provided $Q_A$ is greater than the rate of downgoing flow at the inlet, which is the sum of the net discharge $Q_I$ at the inlet and the rate of reverse flow $Q_{rev}$ there. In this case, however, the amount of sediment offscraped is predictable only as being somewhere between $Q_A - Q_I - Q_{rev}$ and $Q_A - Q_I$, and the amount of melange offscraped is the remaining fraction of $Q_A - Q_I$. The calculations cannot predict type E unambiguously. Instead, if $Q_A \leq Q_I + Q_{rev}$, they can predict only that the type is either D or E, here termed type DE. In this case the amount of sediment offscraped is somewhere between zero and $Q_A - Q_I$, and the amount of melange offscraped is, as before, the remaining fraction of $Q_A - Q_I$.

The five basic types A through E and the composite type DE provide a means of classifying subduction complexes on the basis of seismic reflection profiles and deep-sea drilling results for comparison with the predictions of the model. Their geological and geophysical implications are discussed at length in a separate paper (M. Cloos and R. L. Shreve, unpublished manuscript, 1986).

## APPLICATION TO REPRESENTATIVE SITES

### *Mariana, 18°N: Type A*

This site north of the island of Guam in the western Pacific Ocean has an extremely simple cross section (Figure 5), with no sedimentary rocks, accretionary prism, or forearc high. In this and the other examples presented in this paper, the site is located at or near the named geographic feature at approximately the indicated latitude or longitude, and the line of section extends from the inlet to the volcanic arc in the direction perpendicular to the trench (inasmuch as the model as currently implemented is independent of any component of motion parallel to the trench). The data for this site were compiled from the reports of *Sager* [1980], *Samowitz and Forsyth* [1981], *Hussong and Uyeda* [1982], and *Bloomer* [1983].

The trench axis sediment thickness $h_A$ is roughly 150 m at the site, but may significantly differ elsewhere along the trench. The rate of plate convergence currently is 40 km Ma$^{-1}$ [*Ranken et al.*, 1984, p. 557], and that of backarc spreading is comparable [*Hussong and Uyeda*, 1982, p. 923, Figure 8], making the subduction speed $U$ about 80 km Ma$^{-1}$. From 15 until about 5 Ma ago, however, the spreading rate was much less [*Hussong and Uyeda*, 1982, p. 919, Figure 6], making the subduction speed possibly as slow as 40 km Ma$^{-1}$. Thus it is necessary (and also instructive) to compute a range of cases.

A convenient starting point is to take $U$ to be 40 km Ma$^{-1}$ and $h_A$ to be 150 m (that is, to disregard for the moment the

present backarc spreading). With these values the computed thickness of the subduction channel from the inlet to $X = 120$ km is fairly uniformly about 290 m; from 120 to 170 km it is 315 m; and from there to the volcanic arc it is 360 m (Figure 5). The variations in thickness reflect variations in hydraulic potential gradient $\Phi'$. They can occur in the absence of any downstream decrease in sediment discharge $Q$, such as would be caused by underplating. The steplike nature of the variations (and of all the calculated results) is due to the diagrammatic geometry used in order to limit computing costs; the actual variations would be much smoother. The pattern of flow at the inlet is type A, and no offscraping or reverse flow occurs. The drag $D_H$ on the hanging wall is less uniform than the channel thickness. It is roughly 2.7 MPa (27 bars) as far as 120 km, 1.7 MPa (17 bars) from 120 to 170 km, and about 0.7 MPa (7 bars) beyond, with an average value of 2.0 MPa (20 bars). The drag $D_F$ on the foot wall is approximately 3.5, 3.9, and 4.3 MPa (35, 39, and 43 bars) in the three regions. No underplating occurs, and all incoming sediment is subducted to the volcanic arc. Subduction erosion is favored, but whether or not it actually occurs is beyond the scope of the model. *Hussong and Uyeda* [1982, p. 920] suggested that it may actually have been extensive at this site, but *Bloomer* [1983, p. 7423] suggested erosion only until about 25 Ma ago (early to middle Oligocene), followed by accretion of seamounts; *Karig and Ranken* [1983, pp. 274–275] suggested no significant erosion but instead uplift of a few hundred meters. Of course, accretion of the tops of seamounts could occur concurrently with subduction of their bottoms along with the incoming sediments, or it could even occur concurrently with subduction erosion.

*Bird* [1978] has calculated the average drag on the hanging wall at this site from the requirement that it balance the other forces acting on the overriding block. Considering only the horizontal components of force perpendicular to the trench, these are (1) the normal stress exerted on the foot wall between the inlet and the volcanic arc, which *Bird* [1978, pp. 429–431] calculated from the free air gravity anomaly given by *Watts* [1976] plus a reasonable assumption as to the orientation of the principal stresses near the foot wall; (2) the lithostatic pressure exerted on the back side of the block in the region of backarc spreading in the Mariana Trough (about 150 km behind the volcanic arc); and (3) the hydrostatic pressure exerted by the seawater on the top of the block. *Bird*'s [1978, pp. 412–414, 417] calculation gave a value of 16.5 MPa (165 bars) for the average drag. Recalculation using the density distribution of Figure 5, which accords with the observed free air gravity profile (Figure 5), and *Sager*'s [1980, pp. 5383, 5385] figures for the thickness of the crust and for the anomaly ($-0.033$ Mg m$^{-3}$) in the mantle density in the region of backarc spreading, however, gives a value of only 2.1 MPa (21 bars).

This value agrees well with the 2.0 MPa (20 bars) given by the initial sediment subduction calculation but, as will be seen, is a factor of 3 too low if the present backarc spreading is included. This agreement must be regarded as at least somewhat fortuitous, however, because *Bird*'s [1978] method computes the drag as the difference of two much larger (about 3 orders of magnitude in the recalculated case), nearly equal forces and is therefore extremely sensitive to small differences in the values adopted for some of the parameters. The calculated drag changes by a factor of 2, for example, if the crustal thickness in the region of backarc spreading changes by 5% or

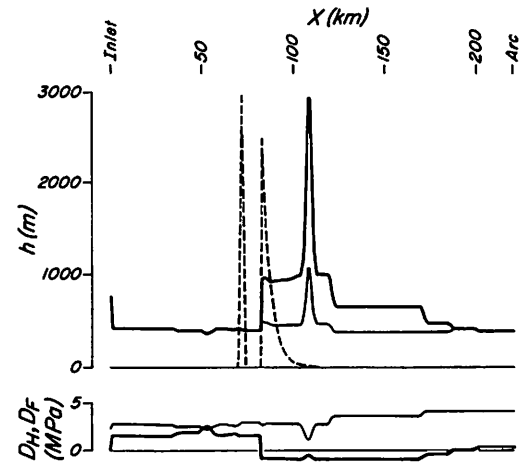


Fig. 6. Mariana, 18°N. $U = 40$ km Ma$^{-1}$; $h_A = 300$ m. The figure corresponds to possible conditions from 15 until about 5 Ma ago, when backarc spreading was small or absent but sediment supply was the same as that at present. The upper graph shows the thickness of the subduction channel (heavy solid curve), the height above which flow is upgoing (light solid curve) in the zone of reverse flow, and the rate of thickening of the overriding block by underplating (dashed curve). The lower graph shows drags on the hanging wall (heavy curve) and foot wall (light curve). Underplating, hence water loss to the hanging wall, occurs in the middle of the zone of serpentinite diapirs found by *Fryer et al.* [1985, p. 774].

the mantle density there changes by only 0.06%. The difference between *Bird*'s [1978] result and the recalculated one is therefore most likely due to the considerably different lithospheric thickness and lithospheric and asthenospheric densities used.

If, keeping $h_A$ at 150 m, $U$ is doubled to 80 km Ma$^{-1}$ (that is, the present backarc spreading is included), the type and the qualitative picture remain unchanged and $h$ changes only slightly, because the dominant process in the subduction channel in this case is the general shearing, but $D_H$ increases by factors of roughly 2, 3, and 6 in the three regions, and $D_F$ nearly doubles. Thus subduction erosion is more probable. If, on the other hand, $U$ is halved to 20 km Ma$^{-1}$, $h$ decreases by 20%, and $D_H$ and $D_F$ by roughly 40%, from the inlet to 90 km and from 185 km to the volcanic arc. In the intervening region a zone of reverse flow appears, in which $h$ ranges from about 300 m to as much as 2000 m; $D_H$ is nearly uniform at about $-0.7$ MPa ($-7$ bars), that is, directed toward the inlet; and $D_F$ is roughly 2.5 MPa (25 bars). At the inlet a combination of less-than-critical $D_H$ and the highly permeable crystalline overriding block causes rapid underplating, which changes the type to B. In fact, approximately 25% of the incoming sediment is underplated at the inlet in this case, and all but a tiny fraction of the rest is subducted to the volcanic arc. With time an accretionary prism would accumulate, so that, as was already noted, the type would eventually evolve to C.

If, keeping $U$ at 40 km Ma$^{-1}$, $h_A$ is halved to only 75 m, the type and the qualitative picture again remain unchanged, with $h$ being uniformly about 140 m and $D_H$ and $D_F$ being about 6.0 and 6.7 MPa (60 and 67 bars). If, on the other hand, $h_A$ is doubled to 300 m (that is, backarc spreading is zero but sediment supply is unchanged, as in the period from 15 until about 5 Ma ago), a zone of reverse flow appears, which originates at 185 km and extends trenchward to the 80-km point, where it peters out (Figure 6). This places the control point at

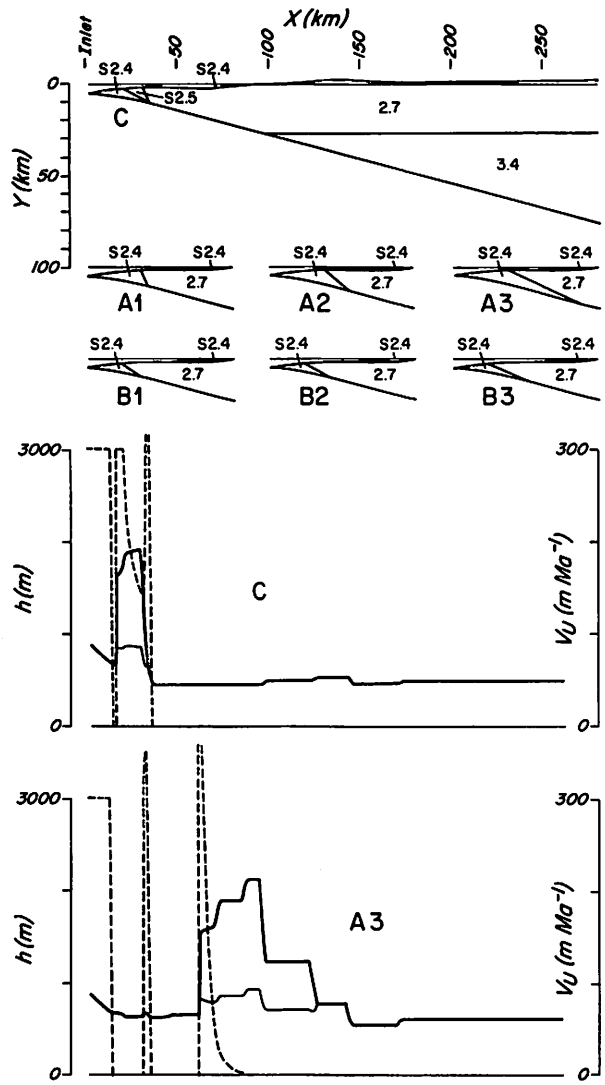


Fig. 7. Late Tertiary Mexico, 17°N, showing seven alternative density cross sections considered. The best choice is probably C. $U = 70$ km Ma$^{-1}$; $h_A = 400$ m. Densities are in megagrams per cubic meter; the prefix S indicates sedimentary rock and the absence of this prefix indicates crystalline rock (or sedimentary rock having density of 2.6 Mg m$^{-3}$ or greater). Graphs show calculated results for alternatives C and A3 (notation is the same as that in Figure 6). The volcanic arc is approximately 365 km from the inlet. The pattern and magnitude of the underplating rate for alternative C closely resemble the pattern and magnitude of the uplift rate inferred from core studies and other data by *Moore et al.* [1982, p. 854].

a depth of 95 km, only 35 km (horizontally) from the center of volcanic arc igneous activity, so the results doubtless are not quantitatively accurate, although they probably are qualitatively correct. Underplating, and hence uplift of the hanging wall and possible serpentinite formation by hydration of some of the overlying rocks, occurs in the trenchward 30 km of the zone of reverse flow and also in a narrow zone near 71 km, where for a short distance the drag locks onto the critical value. These localities occupy the central third of the zone of serpentinite diapirs found by *Fryer et al.* [1985, p. 774]. At the inlet, 5% of the incoming sediment is offscraped and 25% is underplated, making the flow pattern there type C. The drag on the hanging wall changes correspondingly. It is close to 1.5 MPa (15 bars) from the inlet to 80 km, is approximately −1.0 MPa (−10 bars) in the zone of reverse flow, and is zero or nearly so beyond it. The drag on the foot wall, on the other hand, changes only moderately, becoming roughly 3.0 MPa (30 bars) from the inlet to 120 km, 3.7 MPa (37 bars) from 120 to 270 km, and 4.2 MPa (42 bars) beyond.

In general, as this example demonstrates, decreased subduction speed or increased sediment input tends to promote the formation and growth of an accretionary prism. The effects of these variables on channel geometry, flow pattern, underplating rate, and wall drag, however, are not so simply generalized even in cases as simple as this one. Moreover, both accretion and erosion can modify the geometry of the overriding block and downgoing plate, and hence their own patterns, with no change in subduction speed or sediment input.

### *Late Tertiary and Present-Day Mexico, 17°N: Types B and C*

This site near Acapulco on the west coast of southern Mexico has a relatively simple cross section reasonably well constrained except for the thickness of the crystalline continental crust, which does not affect the results, and the position of the arcward boundary, or backstop, of the currently forming, sand-rich accretionary prism, which does. Moreover, core studies from leg 66 of the Deep Sea Drilling Project provide unusually good quantitative information on the evolution of the accretionary prism, from which the late Tertiary geometry of about 4 Ma ago was derived. The data for this site were compiled from the reports of *Fix* [1975], *Moore et al.* [1982], and *Burbach et al.* [1984].

Inasmuch as the backstop in this case separates lower-density, lower-permeability sedimentary rocks from higher-density, higher-permeability crystalline ones, its placement can significantly affect the calculated results. In the case of Mexico, 17°N, seven alternative placements were considered (Figure 7). Alternatives A1, A2, and A3 place the backstop on the arcward side of a "transition zone" [*Moore et al.*, 1982, p. 849] that separates definite accretionary prism rocks from definite continental basement. This placement treats the "transition zone" as part of the prism. Alternatives B1, B2, and B3, on the other hand, place the backstop on the trenchward side, thus treating the "transition zone" as part of the basement. Finally, alternative C, which is probably the best choice, treats the "transition zone" as a separate sedimentary unit of somewhat greater density that may or may not be part of the prism (following *Moore et al.*, [1982, p. 855]).

For the late Tertiary the subduction speed $U$ is taken to be the same as at present, namely 70 km Ma$^{-1}$, whereas the trench-axis sediment depth $h_A$ is assumed to be about 100 m less than at present, or roughly 400 m, to reflect the smaller sediment supply that probably prevailed before the widespread glaciation and sea level lowering of the Quaternary. With these values all seven alternatives give type B flow at the inlet, in agreement with the conclusion of *Moore et al.* [1982, p. 860] that this is a young accretionary prism.

The flow patterns at depth fall into two groups, typified by alternatives A3 and C, that are governed primarily by the differing positions and capacities of the control points. In all seven alternatives, the drag on the foot wall is everywhere less than about 4 MPa (40 bars), and that on the hanging wall is generally about half as great.

Alternative A3 (Figure 7) has a single control point at 123 km, which produces a zone of reverse flow that peters out at 60 km. The diminution of capacity at the control point is due to the trenchward slope of the coastal mountain chain. The

spike in thickening rate at 31 km is due to enhanced underplating caused by water loss through the crystalline rocks. In reality, it would be shifted somewhat trenchward because the water would tend to percolate diagonally upward toward the more permeable rocks. In more mature prisms a spike like this at the backstop would be associated with a forearc high. The necessary conditions are a relatively steep crystalline backstop overlying a relatively shallow subduction channel.

Alternative A2 (not shown) is like A3, except that the reverse flow peters out at 63 km, which because of the somewhat greater depth makes the spike in thickening rate there about a fifth as high. Alternatives B1, B2, and B3 (none shown) are also like A3, except that the spike in thickening rate at 31 km is shifted to 21 km because of the more trenchward position of the backstop.

Alternatives C (Figure 7) and A1 (not shown) have a single control point at 31 km, which produces a zone of reverse flow that peters out at 14 km. Both have a high, narrow spike in thickening rate at 32 km and, like all the alternatives, a uniform thickening rate of about 300 m $Ma^{-1}$ from the inlet to 11 km. Their principal difference, which is due to the difference in treatment of the "transition zone," is in the pattern of thickening from 14 to 29 km: in A1 it is uniform at about 300 m $Ma^{-1}$, whereas in C it decreases more or less uniformly from this figure to about 140 m $Ma^{-1}$.

The overall pattern and magnitude of thickening rate calculated for alternative C closely resembles that of the uplift rates inferred from core studies and other data by *Moore et al.* [1982, p. 854], after allowance for isostatic adjustment. The principal differences are the spike between 30 and 33 km and the gap between 11 and 14 km. Decreasing the permeability used for the crystalline rocks to a fifth the adopted value, which is entirely reasonable in light of the observed variability of this property, would eliminate the spike. Likewise, increasing the trench axis sediment thickness very slightly, to 410 m, would just eliminate the gap; and increasing it further would cause offscraping of the excess sediment at the inlet.

With the present-day sediment supply ($h_A = 500$ m) and geometry (Figure 8; note that the inlet, and hence the coordinate system, has moved 4 km trenchward in relation to the overriding block since the late Tertiary) the flow at the inlet is type C. Approximately 12% (or roughly 4 $km^2$ $Ma^{-1}$) of the incoming sediment is offscraped, which is about a third of the amount underplated. Decreasing $h_A$ to 440 m would reduce offscraping to zero (and change the type to B). The zone of reverse flow as well as the pattern and magnitude of the thickening due to underplating and of the drag on the foot wall are unchanged from the late Tertiary.

The calculated results thus agree well with the observations of *Moore et al.* [1982] as regards offscraping and thickening, and they concur as regards the importance of underplating. They indicate that the rocks beneath the zone of landward dipping reflectors consist of underplated subduction melange. This explains the lack of coherent acoustic returns from this part of the prism noted by *Moore et al.* [1982, p. 854], because such melange undergoes complex and intense deformation when it reverses direction in the subduction channel. They also indicate that the zone of landward dipping acoustic reflectors that underlies the upper 2 to 3 km of the prism consists principally of underplated, rather than offscraped, sediment. This suggests that the reflectors may be sedimentary beds, as *Moore et al.* [1982, p. 853] surmised. The longer, more continuous reflectors may be due to systematic alignment of beds near relict thrust faults inherited from the zone of compression and the inlet of the channel, inasmuch as during underplating (or weak offscraping) the thrust faults approximately parallel the hanging wall and hence are deactivated and accreted over relatively long lengths all at once. During stronger offscraping, however, their offscraped portions do not parallel the accretion front and hence tend to be deactivated and accreted piecemeal, which disrupts their continuity (further details and possible exceptions are given by M. Cloos and R. L. Shreve (unpublished manuscript, 1986)). This explains why prominent landward dipping reflectors are scarce in most accretionary prisms, because they would form only where the flow at the inlet is type B (or type C with little offscraping), as at Mexico, 17°N.

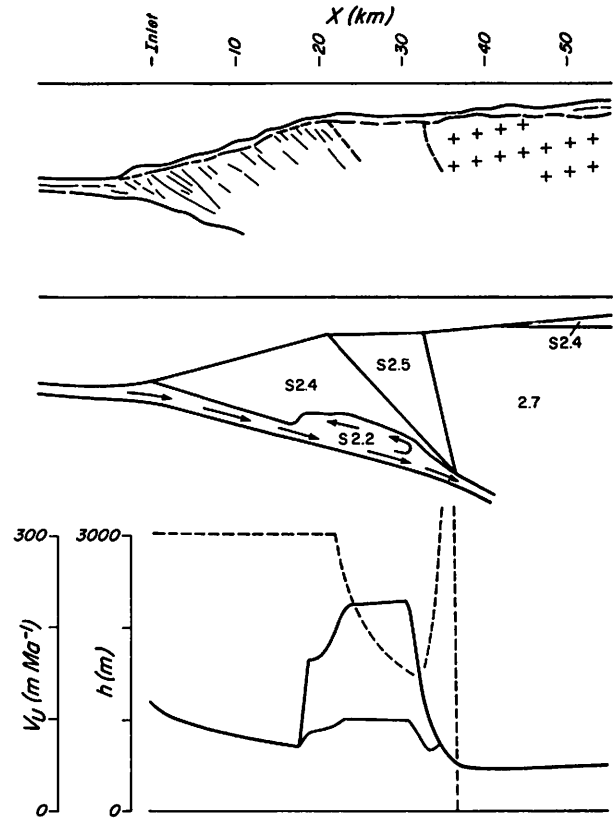


Fig. 8. Present-day Mexico, 17°N. $U = 70$ km $Ma^{-1}$; $h_A = 500$ m. The upper cross section is after *Moore et al.* [1982, p. 849, Figure 2]. The lower one was used in the calculation (notation is the same as that in Figure 7). Vertical exaggeration is 2× in both cross sections. The graph shows the calculated results (notation is the same as that in Figure 6). Recalculation taking into account the geometry of the subduction channel changes the results only slightly. The landward dipping acoustic reflectors are in underplated sedimentary beds, as *Moore et al.* [1982, p. 853] surmised; the longer, more continuous reflectors may be due to systematic alignment of beds near relict thrust faults inherited from the zone of compression. The underlying acoustically incoherent region reported by *Moore et al.* [1982, p. 854] is underplated subduction melange, whose coherence is destroyed by the intense deformation when it reverses direction in the subduction channel.

*Lesser Antilles, 13°N (Barbados): Type C*

This site at the island of Barbados, 190 km east of the Lesser Antilles arc between the western Atlantic Ocean and the southern Caribbean Sea, is notable for its slow subduction speed and thick blanket of incoming sediment. The data for it

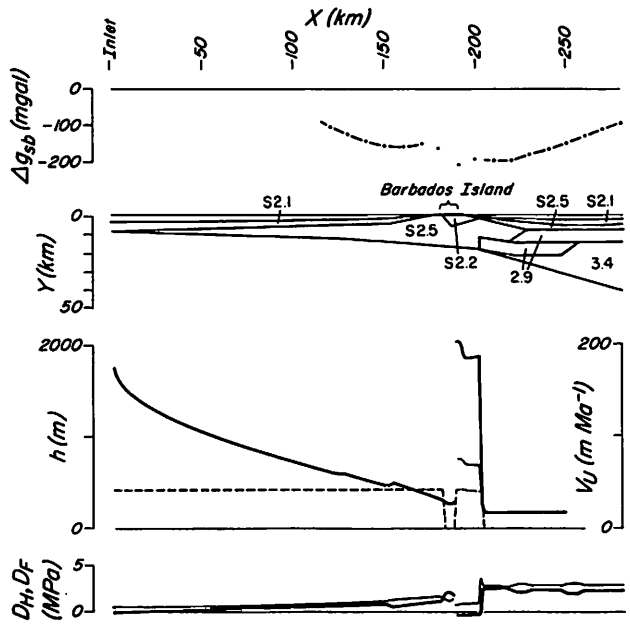


Fig. 9. Lesser Antilles, 13°N (Barbados). $U = 20$ km Ma$^{-1}$; $h_A = 4000$ m; trench axis sediment density $\rho_A = 2.1$ Mg m$^{-3}$ (nonstandard value). Although it is included in the calculation, the portion of section from 280 km to the volcanic arc at 360 km is omitted to save space. The graph above the density cross section (notation is the same as that in Figure 7) shows the observed (broken heavy curve [*Westbrook*, 1975, p. 219]) and calculated (dots; assumptions are the same as those for Figure 5) simple Bouguer gravity anomaly computed for a correction density of 2.1 Mg m$^{-3}$. The graphs below the cross section show the calculated results (notation is the same as that in Figure 6). Accumulation arcward of a short zone of unlimited capacity beneath Barbados Island produces diapiric upwelling of subduction melange as *Speed and Larue* [1982, p. 3641] postulated.

were compiled from the reports of *Westbrook* [1975], *Speed and Larue* [1982], *Stein et al.* [1982], and *Westbrook and Smith* [1983].

The subduction speed is about 20 km Ma$^{-1}$. No trench in the usual sense is present. Instead, the relatively flat abyssal plain turns upward along a sharp deformation front, where compression of the sediment blanket begins, about 250 km trenchward of the island and roughly 50 km from the inlet. The sediment, which is mud-rich (in relation to that at such sites as Mexico, 17°N, or Alaska, 153°W) and carbonate bearing, is about 4000 m thick at the front and 5000 m thick at the inlet, where much of it appears to be offscraped. Both thicknesses decrease considerably from south to north and may have changed significantly with time, as the relationship of the Caribbean plate changed in relation to the mouth of the Orinoco River. The sediment density $\rho_s$ in the subduction channel is taken to have the standard value, 2.2 Mg m$^{-3}$, whereas its density $\rho_A$ at the deformation front has the value 2.1 Mg m$^{-3}$ [*Westbrook*, 1975, p. 226], instead of the standard 2.0 Mg m$^{-3}$.

Barbados Island is a prominent high on the forearc ridge, which elsewhere is a broad, irregular swell 1500 m or more below sea level. The island is underlain by a basal complex of highly faulted and folded sedimentary units of Paleocene through late Eocene age that were incorporated into the accretionary prism after accumulation on the sea floor [*Speed and Larue*, 1982, pp. 3637–3638, 3641–3642]. Overlying the basal complex in low-angle fault contact are the Oceanic and Bissex Hill nappes, which consist of pelagic sedimentary units of middle Eocene through Miocene age that probably were deposited on the arcward flank of the early accretionary prism [*Speed and Larue*, 1982, pp. 3635–3637, 3641; D. K. Larue, personal communication, 1985]. The island is capped by Pleistocene reefs that were arched upward during the last 0.6 to 0.7 Ma at rates ranging from 200 m Ma$^{-1}$ to a maximum of 450 m Ma$^{-1}$ near the center of the island [*Speed and Larue*, 1982, pp. 3634–3635]. *Speed and Larue* [1982, p. 3641] suggested that this arching and the considerable later Tertiary uplift of the island were due to diapiric upwelling of subducted sediments.

The sedimentary units in the forearc basin arcward of the island reach a total thickness of 6 to 7 km [*Westbrook*, 1975, p. 226]. They are relatively undisturbed near the center of the basin but are folded and separated by angular unconformities toward the crest of the forearc ridge [*Westbrook*, 1975, p. 208]. Inasmuch as the lowermost of these units probably correlate with the rocks of the Oceanic and Bissex Hill nappes, this folding and the nappe formation may well be due to the same tectonic episode.

The cross section used as input (Figure 9) was drawn to accord with these facts and interpretations. For the most part, it also closely follows the geophysical interpretations of *Westbrook* [1975], which were constructed to fit the gravity profile in light of the seismic and magnetic data. From the standpoint of the calculations, the two most important features are the wedge of rock with density of 2.2 Mg m$^{-3}$ beneath Barbados Island and, as usual, the backstop.

The wedge replaces the thinner layer of lighter rock shown capping the island by *Westbrook* [1975, p. 226]. It is intended to represent the sedimentry diapirs postulated by *Speed and Larue* [1982, p. 3641] and, although the diapirs probably exist as multiple bodies at various relatively shallow depths, is drawn at the top of the section simply for convenience, because all that counts in the subduction calculation is the total weight of the column of rock overlying the channel. The basis for the details of its geometry are discussed farther on.

The general placement and geometry of the backstop follows the density distribution at depth deduced by *Westbrook* [1975, p. 226]. The specific details, however, are definitely speculative. The idea is that the doubling of the oceanic crust between 216 and 255 km occurred by arcward underthrusting of crust after accretion of a small prism and deposition of the rocks of the Oceanic and Bissex Hill nappes. Compression of the relatively weak forearc basin sediments across this break caused uplift (or further uplift) of the forearc ridge, folding of the sedimentary cover on its arcward flank, and trenchward thrusting of the nappes (probably only a short distance and perhaps facilitated by high pore pressures due to the compression).

From the standpoint of the subduction calculation, however, the only critical detail of the backstop is the leading edge of oceanic crust at 200 km. Such a steep contact between such contrasting densities so near the subduction channel will produce a control point of extremely low capacity. The cubic splines smoothing of the hydraulic gradient $\Phi'$, however, severely attenuates or even completely eliminates the effects of such narrow features. For just this one feature, therefore, the computer program was temporarily modified to eliminate the smoothing and instead to calculate $\Phi'$ as if the transition zone between the accretionary prism and the oceanic crust were 2 km wide. The transition could consist of gradation of one rock to the other over this distance, inclination of the contact 2 km

either way over its 7-km height, or some equivalent combination.

The calculated results (Figure 9) show that the capacity of the inlet is only about 15% of the sediment supply. Thus 85% is offscraped. About 11% is uniformly underplated between the inlet and Barbados Island, producing a thickening rate of 40 m $Ma^{-1}$. No underplating occurs beneath the trenchward part of the island, which is a zone of unlimited capacity. The control point at the backstop at 200 km produces a zone of reverse flow that extends to the arcward end of this zone, where subduction melange accumulates at a rate of 0.6 $km^2$, $Ma^{-1}$ or about 1% of the total sediment supply. This localized accumulation of lower-density melange in turn produces the diapiric upwelling beneath Barbados Island postulated by *Speed and Larue* [1982, p. 3641]. This upwelling differs in both mechanism and scale from the mud volcanism reported by *Westbrook and Smith* [1983]. Finally, another 1% of the sediment supply is underplated in the zone of reverse flow; and the remaining 2% is subducted to the volcanic arc.

If the smoothing at 200 km were retained, the results would not change trenchward of the zone of unlimited capacity. Arcward of it, however, the control point would shift to 317 km, the resulting zone of reverse flow would peter out 13 km short (arcward) of the zone of unlimited capacity, and thus diapiric upwelling of melange would not occur. About 3% of the sediment suppy would be subducted to the volcanic arc.

With the smoothing at 200 km omitted, the drag on the foot wall is less than about 1.5 MPa (15 bars) from the inlet to the backstop at 200 km and is approximately 3.0 MPa (30 bars) from there to the volcanic arc, in agreement with the almost total lack of earthquakes trenchward of Barbados Island and with the low magnitudes (all less than 5) of the few arcward of it [*Stein et al.*, 1982, p. 8643].

Increased or decreased sediment supply does not change these results, except for the amount of sediment offscraped, unless the supply falls below the inlet capacity, which is extremely unlikely. Decreased permeability of the sedimentary rocks decreases the rates of underplating and thickening and drastically increases the rates of melange accumulation and diapirism beneath the island. A decrease of only 6%, for example, doubles the rate of accumulation. Likewise, increased permeability can decrease it to zero by causing the reverse flow to peter out before reaching the zone of unlimited capacity. Increased subduction speed, however, increases the rate of melange accumulation and diapirism. An increase of 5%, to 21 km $Ma^{-1}$ for example, more than doubles it, to 1.4 $km^2$ $Ma^{-1}$. An increase of 10% does not more than quadruple it, however, but only triples it, because a second control point develops at 152 km, which limits the amount of sediment reaching the backstop (and also produces a zone of reverse flow that reaches the inlet and changes the type to D). A decrease of 5% in the subduction speed, on the other hand, reduces the rate of melange accumulation and diapirism nearly to zero.

Without the zone of unlimited capacity the reverse flow from the backstop would extend to the inlet, the type would be D instead of C, and no melange would accumulate beneath the island. The existence of the zone, however, is due to the presence of the wedge of diapirically emplaced low-density melange. Thus some other mechanism must have initiated the diapirism. The most likely possibility is formation of an arcward facing surface slope a few kilometers long just trenchward of the backstop. Because of the very small gradient of the subduction channel in this vicinity, the minimum necessary surface gradient would have been no more than about 65 m $km^{-1}$ (or 30 m $km^{-1}$ if a tapering sedimentary cover comparable to the present one were present), which could easily have been produced by differential uplift in the same event that produced the folds and nappes.

The newly initiated diapirism had two effects on $\Phi'$ and hence on the zone of unlimited capacity. At the arcward end of the zone it made $\Phi'$ more positive by decreasing (or even reversing) the surface slope there, whereas just trenchward of the end it made $\Phi'$ more negative by introducing a horizontal gradation in density without a fully compensating change in surface gradient. Thus the zone of unlimited capacity and the locus of diapiric intrusion migrated trenchward, continuing even where $\Phi'$ was originally positive, until stopped by a sufficiently adverse surface gradient or density contrast, and it left behind a zone of very small positive $\Phi'$. The base of the wedge of diapirically intruded rock beneath Barbados Island shown on the cross section (Figure 9) was therefore drawn so as to make $\Phi'$ small and positive from the present locus of intrusion at 185 km to the initial one at 200 km. From 185 to 180 km it was drawn to reflect the likely lateral dispersion of the rising diapirs.

The cross-sectional area of this wedge is 66 $km^2$. Accumulation of this volume at 0.6 $km^2$ $Ma^{-1}$ would take 110 Ma, which is somewhat more than twice as long as the maximum time available (namely, since the middle Eocene). Over the long term, however, the accumulation rate must have decreased as the accretionary prism grew and diverted more and more sediment to underplating. If the pre-Quaternary sediment supply were, say, roughly 75% of the present value, as seems likely, the accretionary prism would have grown trenchward about 125 km in the last 20 Ma, the rate of melange accmulation in that period would have dropped from 6 $km^2$ $Ma^{-1}$ to its present value, and the total accumulation would have been approximately 66 $km^2$, as is required.

These calculations indicate a long-term average uplift rate due to diapiric intrusion beneath Barbados Island of the order of 30 m $Ma^{-1}$ and a present average rate an order of magnitude less (assuming a 30-km-long zone of uplift). Even the long-term rate is about an order of magnitude less than the documented Pleistocene rate. The explanation lies in the fact that the formation of diapirs at the subduction channel is not a continuous process. Instead, sufficient melange must accumulate between the formation of one diapir and the next to bring on instability, at which point the diapir detaches from the channel and rises to the surface, where a pulse of uplift signals its arrival. Thus the calculations support the suggestion of *Speed and Larue* [1982, p. 3641] that the Pleistocene uplift of the island must be such a pulse.

*Alaska, 153°W (Kodiak): Type C*

At this site at Kodiak Island off the coast of southwestern Alaska the remains of an older accretionary prism of Cretaceous and early Tertiary age forms the backstop for the present-day prism. The data for the site were compiled from the cross section of *von Huene et al.* [1979] and the reports of *Shor and von Huene* [1972], *von Huene* [1979], *Davies and House* [1979], *Reyners and Coles* [1982], *Fisher et al.* [1983], and *House and Jacob* [1983].

The subduction speed is about 60 km $Ma^{-1}$. The trench fill is about 1600 m thick and consists almost entirely of sand-rich turbidites rather than pelagic or hemipelagic sediments. The

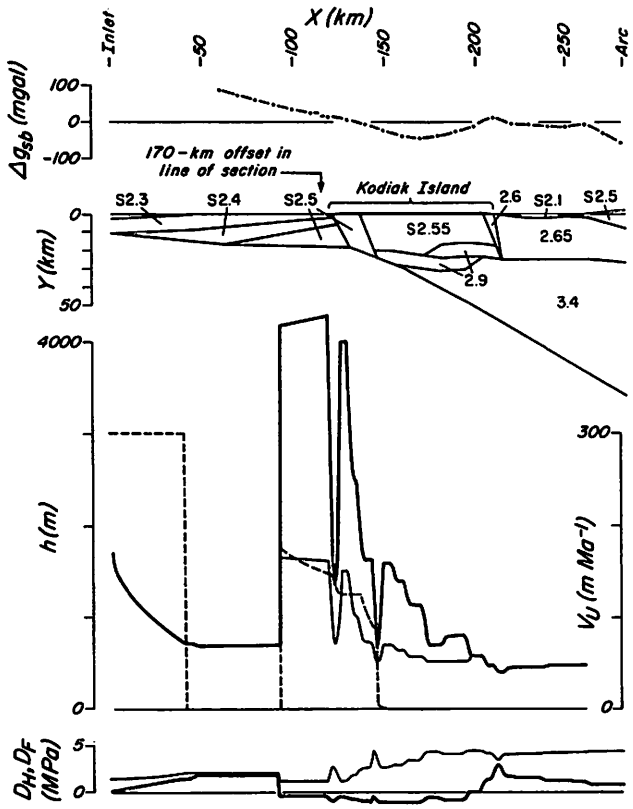


Fig. 10. Alaska, 153°W (Kodiak). $U = 60$ km Ma$^{-1}$; $h_A = 1600$ m. The graph above the density cross section (notation is the same as that in Figure 7) shows the observed (broken heavy curve [*von Huene et al.*, 1979, map] and calculated (dots; assumptions are the same as those for Figure 5) simple Bouguer gravity anomaly computed for a correction density of 2.67 Mg m$^{-3}$. The graphs below the cross section show the calculated results (notation is the same as that in Figure 6). The drag on the foot wall is relatively low trenchward of Kodiak Island and high arcward of it, which accords with the distribution of earthquake hypocenters [*von Huene*, 1979, p. 270; *von Huene et al.*, 1979]. Blocks detached from the hanging wall in a region of reverse flow, such as that beneath Kodiak Island, sink into matrix that reversed direction at progressively higher levels. This explains the "exotic" blocks of blueschist or eclogite from depths of 25 km found in melange whose matrix has not gone to depths greater than about 10 km.

inlet, which is about 40 km arcward of the trench axis, and the structural units within the present-day prism are placed (Figure 10) in accordance with the seismic velocity boundaries inferred by *Shor and von Huene* [1972, p. 699] and *von Huene et al.* [1979]. The steeply inclined blocks below the trenchward and arcward edges of Kodiak Island are drawn to reflect known surface faults.

The structure beneath the rest of the island is not well constrained. The doubling of the oceanic crust (density of 2.9 Mg m$^{-3}$) is drawn to account for the considerable shortening needed to produce the isoclinal folding of the overlying sedimentary rocks [*von Huene et al.*, 1979, p. 3], and its depth and geometry are chosen to reproduce the measured simple Bouguer gravity anomaly (Figure 10) [*von Huene et al.*, 1979, map]. The top of a similar structure (or possibly the same one) may be the deep acoustic reflector detected at a depth of 13 to 14 km approximately 170 km along strike to the northeast by *Fisher et al.* [1983, p. 5847].

The calculated results show that about 61% of the incoming sediment is offscraped at the inlet, 16% is underplated in the first 40 km, 10% is underplated as melange between 92 and about 145 km, and the remaining 13% is subducted to the volcanic arc. The pattern of thickening due to underplating (Figure 10) agrees fairly well with the pattern of uplift of the trench slope, downwarping of the shelf, uplift in the vicinity of the trenchward side of Kodiak Island, and downwarping just arcward of it suggested by the topography and by the seismic reflection profiles [*von Huene et al.*, 1979]. The actual rate of thickening beneath the trench slope relative to that beneath the island should be much greater than the rate calculated, however. Increasing the density of the lowermost unit of the present-day prism from 2.5 to 2.6 Mg m$^{-3}$ would remove this discrepancy, but such a high density seems atypical in comparison with that of other accretionary-prism rocks elsewhere, and it requires highly improbable changes in the rest of the structure in order to fit the observed gravity profile. A much more likely possibility is that the part of the prism beneath the trench slope undergoes longitudinal compression, as analyzed by *Davis et al.* [1983] and by *Stockmal* [1983], that significantly increases its thickness as it grows forward. Clearly, such a mechanism must be important wherever a relatively bluntly tapered prism grows primarily by offscraping, as in this case.

The control point is located 194 km from the inlet, beneath the arcward part of Kodiak Island. It allows only about 12 km$^3$ Ma$^{-1}$ of sediment per kilometer of trench to be subducted to the volcanic arc and produces a zone of reverse flow that peters out 100 km to trenchward (Figure 10). These quantities are governed almost entirely by the inclination of the base of the oceanic crust at the arcward end of the doubled region. A shallower inclination would shift the control point trenchward to the leading edge of the oceanic crust at 143 km but would otherwise have little effect, inasmuch as the capacity at 143 km exceeds that at 194 km by only 2.5%. Eliminating the cubic splines smoothing at the leading edge, as for Barbados Island, also shifts the control point to 143 km but has little other effect, because it decreases the capacity by only 4%. Eliminating both the doubling and the steep leading edge of the oceanic crust shifts the control point arcward all the way to 262 km but again has little effect because the capacity there is only 2.5% greater than that at 194 km. Thus the calculated results in this case are largely insensitive to the uncertainties in the structure of the site.

Practically no reverse flow passes the point of very low local capacity at 143 km. The bulk of the melange between this point and the control point at 194 km therefore simply cycles up and down in a whirlpoollike gyre. The tiny amount of melange that is underplated near the upper end of this region rises 25 km (pressure drop of 800 MPa, or 8 kbar) from depths of approximately 50 km (pressure of 1400 MPa, or 14 kbar). A second gyre is located between 143 km and a point of moderately low local capacity at 121 km. A significant amount of the melange in this gyre is lost to the hanging wall by underplating, so that only the core of the gyre cycles up and down. The presence of this core, however, means that the underplated melange all comes from near 143 km, rising a maximum of 5 km (pressure drop of 150 MPa, or 1.5 kbar, from 600 MPa, or 6 kbar). In addition, some melange from this zone passes 121 km and makes it arcward as far as 104 km (pressure of 420 MPa, or 4.2 kbar) before all of it is underplated. The sediment that reverses direction near 121 km is underplated between 104 and 92 km, rising a maximum of only 0.8 km. Thus the distance melange rises (and the pressure drop it experiences) before incorporation into the accretionary prism is governed

mainly by the arrangement of gyres and the rate of underplating.

Blocks detached from the hanging wall in a region of reverse flow, such as that beneath Kodiak Island, will be carried arcward by the upgoing melange. To be carried far, their size and density must be such that they sink faster than the rate of underplating but slower than the vertical motion of the matrix. Thus they sink into matrix that reversed direction at progressively higher levels. This explains the "exotic" blocks of blueschist or eclogite from depths of 25 km found in melange whose matrix has not gone to depths of greater than about 10 km.

The drag on the foot wall increases from about 1.5 MPa (15 bars) at the trenchward edge of Kodiak Island to about 4.5 MPa (45 bars) near the middle of the island. To arcward and trenchward of this region it is relatively uniform at about 4.5 and 1.5 MPa (45 and 15 bars). This pattern accords with the observation [*von Huene*, 1979, p. 270; *von Huene et al.*, 1979] that from the trench to the island the earthquake hypocenters are widely scattered (some even being below the crust, which suggests they are probably due to bending of the descending plate), whereas farther arcward they are well clustered within a 15-km-thick Benioff zone (which suggests they are due to drag on the top of the descending plate). Moreover, the magnitude of the drag in the arcward region accords with the stress drops of 2 to 6 MPa (20 to 60 bars), typical of large thrust-type earthquakes in subduction zones [*Kanamori*, 1977, p. 2983], assuming that the stress drops are a substantial fraction of the total stress acting, as seems probable where saturated sediments are subducted and pore pressures therefore approach the lithostatic pressure.

*Late Tertiary and Present-Day Japan, 40°N: Types A and DE*

This site on the east coast of Honshu, the chief island of Japan, is noteworthy for its extensive mud-rich Cretaceous accretionary prism, which backstops a much smaller present-day one. The data for it were compiled from the reports of *Sugimura and Uyeda* [1973, p. 29], *Hasegawa et al.* [1978], and *von Huene et al.* [1982].

The subduction speed is 100 km $Ma^{-1}$, and the thickness of sediment at the trench axis is about 500 m. The present-day backstop is only about 30 km from the trench axis [*von Huene et al.*, 1982, p. 831]. For lack of better information the inlet is placed halfway between the two (Figure 11). It could almost as plausibly be placed as much as 10 km to either side, however, without significantly altering the calculated results.

*Von Huene et al.* [1982, p. 843] concluded that the present-day backstop must have undergone subduction erosion during the latter part of the Tertiary. Thus it probably dips relatively gently arcward and, in the absence of any direct evidence, is drawn approximately parallel to the deeper seismic reflectors in the vicinity [*von Huene et al.*, 1982, p. 834, section JNOC-2]. Because of the small density contrast across it, its exact inclination is not critical.

The Cretaceous prism is approximately 200 km wide. Unconformably overlying almost its entire width is a blanket of gently dipping Miocene and younger sediments about 2 km thick. Near its arcward margin a deep synclinorium about 70 km across affects strata as young as Oligocene [*von Huene et al.*, 1982, pp. 839–840]. On the cross section (Figure 11) the crust is drawn to reflect this feature, guided by the downwarping and downfaulting observed at Mariana, 18°N [*Hussong and Uyeda*, 1982, p. 911]. As will be seen, the details of this structure have no significant effect on the calculated results.

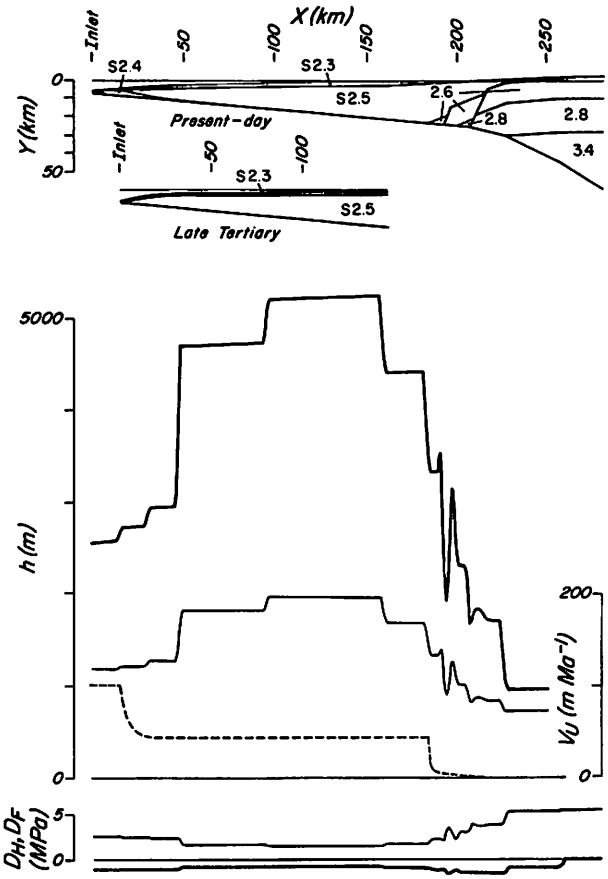


Fig. 11. Present-day Japan, 40°N, with inset showing late Tertiary cross section (notation is the same as that in Figure 7). $U$ = 100 km $Ma^{-1}$ $h_A$ = 500 m at present and 375 m in the late Tertiary. The graphs show the calculated results (notation is the same as that in Figure 6). The control point is at 256 km, and the volcanic arc is at 340 km. The subduction channel is 2.5 km thick at the inlet and 4 to 5 km thick over a 150-km reach beneath the extensive Cretaceous accretionary prism. At present, melange or melange overlain by sediment is being offscraped onto the small present-day accretionary prism. During the late Tertiary, however, no material was being offscraped at the inlet or underplated in the first 20 km of the channel, in agreement with the conclusion of *von Huene et al.* [1982, p. 843] that in fact subduction erosion of the present-day backstop was probably occurring then.

For the present-day data these results (Figure 11) show that about 8 $km^2$ $Ma^{-1}$ of incoming sediment and returning melange are offscraped, but because the type is DE, the calculation cannot give the proportion of each. A zone of reverse flow reaches clear to the inlet from a control point at 256 km. Thus the material being underplated, which totals about 11 $km^2$ $Ma^{-1}$, is everywhere melange, which according to the calculation originated at depths greater than 25 km (or pressure greater than 600 MPa, or 6 kbar). The channel is 2000 to more than 5000 m thick from the inlet to 205 km. The drag on the hanging wall is low from the inlet to about 200 km, increases to nearly 6 MPa (60 bars) at 225 km, and is approximately uniform from there to the volcanic arc, in fair agreement with the observed distribution of earthquakes [*Hasegawa et al.*, 1978, p. 48]. About 27 $km^2$ $Ma^{-1}$ of sediment, or approximately 58% of the total supply at the trench, passes the control point and is subducted to the volcanic arc.

The late Tertiary cross section is drawn by removing the present-day prism and downdropping the trenchward end of the Cretaceous one accordingly (Figure 11, inset). In addition, the thickness of sediment at the trench axis is taken to be 375 m, which is 75% of the present-day value. The calculated results show a zone of reverse flow that arises from the same control point as at present but peters out about 20 km from the inlet. No underplating occurs between this point and the inlet, and there is no offscraping. Thus the results indicate possible subduction erosion of the present-day backstop preceding the current episode of offscraping, in agreement with the conclusion of *von Huene et al.* [1982, p. 843].

Increasing the sediment supply narrows the zone of possible erosion. When the trench axis sediment thickness reaches 380 m in a quasi-steady state, the drag on the hanging wall falls below 1.5 MPa (15 bars) at the inlet, the possible erosion becomes underplating, and the type changes from A to B. When the thickness reaches 385 m, offscraping begins, and the type changes to DE. In actuality, of course, events at the inlet will lag behind changes in sediment supply. A crude estimate of the timing can be made by comparing the excess supply of sediment with the volume of the present-day prism and the changes in calculated steady state volumes of the subduction channel and compressional zone. Assume, for example, that after reaching 385 m at a certain time to be determined, the trench axis sediment thickness increased linearly, reaching 500 m about 2 Ma ago and then remaining constant until the present. The comparison of volumes indicates that the sediment thickness reached 385 m about 14.7 Ma ago (early middle Miocene) but that offscraping, and hence accretion of the small present-day prism, did not begin until 5.3 Ma ago (latest late Miocene). A corollary result is that the accreted layer of offscraped material is 2.8 km thick. These results agree with the data currently available from seismic reflection profiling and deep-sea drilling of this accretionary prism.

## CONCLUSION

These examples illustrate the diverse ways that sediment subduction takes place in different situations, and they demonstrate the impossibility of straightforward generalization from only a few sites, however well studied. They also demonstrate the power of the proposed model, even though still rather crudely implemented, to predict and to explain a wide variety of geological and geophysical features of subduction zones, and they direct attention to the specific observations and measurements most important to further progress. Three areas for improvement particularly stand out: (1) the geometry and properties of the overriding block, especially the backstop (or, more generally, the control point); (2) the large-scale permeabilities of rock and sediment in place and at depth; and (3) the density and rheological properties of the sediment and melange in the subduction channel. Although the present implementation reflects the need for maximum possible simplicity in this initial exploration of the model as well as the lack of better information, it can readily be modified to reflect improvements in any of these areas. The flow in the channel, for example, could be computed using a power law or other viscosity (at the cost of considerably increased computation), or even nonlinear Bingham behavior [*Prager*, 1961, pp. 136–138], provided the necessary material parameters were known. Likewise, the potential water loss, the underplating cutoff, and the subduction channel pressure could all be computed more realistically were better information available. Nevertheless, even in its present implementation the model appears to go far toward a comprehensive quantitative understanding of the dynamics of sediment subduction, melange formation, and prism accretion.

## NOTATION

This list does not include symbols that are only used near where they are defined.

$C_G$, $C_L$ global and local capacities of subduction channel, $km^2\ Ma^{-1}$.
$D_F$, $D_H$ drags on foot wall and hanging wall, MPa.
$D_{HC}$ critical drag on hanging wall for cutoff of underplating, MPa.
$g$ acceleration due to gravity, $m\ s^{-2}$.
$h$ thickness of subduction channel, m.
$h'$ derivative of $h$ with respect to $x$, $m\ km^{-1}$.
$h_A$ thickness of sediment fill at trench axis, m.
$p_H$ pressure in subduction channel, MPa.
$Q$ net discharge of sediment in subduction channel, $km^2\ Ma^{-1}$.
$Q_A$ supply of incoming sediment at trench axis, $km^2\ Ma^{-1}$.
$q_w$ volume rate of water loss to unit area of hanging wall, $m\ Ma^{-1}$.
$U$ speed of subduction, $km\ Ma^{-1}$.
$V_H$ component of velocity of imminently underplated sediment or melange toward hanging wall, $m\ Ma^{-1}$.
$V_U$ thickness of new rock underplated onto hanging wall in unit time, $m\ Ma^{-1}$.
$X$ Cartesian coordinate measured horizontally arcward from inlet, km.
$Y$ Cartesian coordinate measured vertically downward from sea level, km.
$x$ curvilinear coordinate measured arcward along foot wall from inlet, km.
$y$ curvilinear coordinate measured upward perpendicular to foot wall, m.
$\alpha$ dimensionless flow parameter (equation (8*b*)).
$\kappa$ dimensionless subduction channel thickness (equation (8*a*)).
$\mu_s$ viscosity of subducting sediment and returning melange, Pa s.
$\mu_w$ viscosity of water, mPa s.
$\rho_A$ density of sediment fill at trench axis, $Mg\ m^{-3}$.
$\rho_s$ density of subducting sediment and returning melange, $Mg\ m^{-3}$.
$\rho_w$ density of water, $Mg\ m^{-3}$.
$\Upsilon$ dimensionless sediment discharge (equation (8*a*)).
$\Upsilon_I$ dimensionless sediment discharge at inlet.
$\Phi$ hydraulic potential in subduction channel, MPa.
$\Phi'$ derivative of $\Phi$ with respect to $x$, $MPa\ km^{-1}$.

*Acknowledgments.* We thank W. M. Bruner, D. K. Larue, J. C. Moore, and N. H. Sleep for valuable discussion and criticism. Publication of this paper was supported in part by the National Science Foundation, grant EAR85-17272. University of California, Los Angeles, Institute of Geophysics and Planetary Physics publication 2642; University of Texas Institute for Geophysics contribution 641.

## REFERENCES

Aoki, Y., T. Tamano, and S. Kata, Detailed structure of the Nankai Trough from migrated seismic section, *Mem. Am. Assoc. Pet. Geol.*, *34*, 309–324, 1983.

Bally, A. W., Thoughts on the tectonics of folded belts, *Spec. Publ. Geol. Soc. London, 10*, 13–32, 1981.

Batchelor, G. K., *An Introduction to Fluid Dynamics*, 615 pp., Cambridge University Press, New York, 1967.

Bird, P., Stress and temperature in subduction shear zones: Tonga and Mariana, *Geophys. J. R. Astron. Soc., 55*, 411–434, 1978.

Bloomer, S. H., Distribution and origin of igneous rocks from the landward slopes of the Mariana Trench: Implications for its structure and evolution, *J. Geophys. Res., 88*, 7411–7428, 1983.

Brace, W. F., Permeability of crystalline and argillaceous rocks, *Int. J. Rock Mech. Min. Sci. Geomech. Abstr., 17*, 241–251, 1980.

Bray, C. J., and D. E. Karig, Porosity of sediments in accretionary prisms and some implications for dewatering processes, *J. Geophys. Res., 90*, 768–778, 1985.

Bryant, W. R., W. Hottman, and P. Trabant, Permeability of unconsolidated and consolidated marine sediments, Gulf of Mexico, *Mar. Geotechnol., 1*, 1–14, 1975.

Burbach, G. V., C. Frolich, W. D. Pennington, and T. Matumoto, Seismicity and tectonics of the subducted Cocos plate, *J. Geophys. Res., 89*, 7719–7735, 1984.

Carter, N. L., Steady state flow of rocks, *Rev. Geophys., 14*, 301–360, 1976.

Cloos, M., Flow melanges: Numerical modeling and geologic constraints on their origin in the Franciscan subduction complex, California, *Geol. Soc. Am. Bull., 93*, 330–345, 1982.

Cowan, D. S., and R. R. Silling, A dynamic scaled model of accretion at trenches and its implications for the tectonic evolution of subduction complexes, *J. Geophys. Res., 83*, 5389–5396, 1978.

Dahlen, F. A., Noncohesive critical Coulomb wedges: An exact solution, *J. Geophys. Res., 89*, 10,125–10,133, 1984.

Dahlen, F. A., J. Suppe, and D. Davis, Mechanics of fold-and-thrust belts and accretionary wedges: Cohesive Coulomb theory, *J. Geophys. Res., 89*, 10,087–10,101, 1984.

Davies, J. N., and L. House, Aleutian subduction zone seismicity, volcano-trench separation, and their relation to great thrust-type earthquakes, *J. Geophys. Res., 84*, 4583–4591, 1979.

Davis, D., J. Suppe, and F. A. Dahlen, Mechanics of fold-and-thrust belts and accretionary wedges, *J. Geophys. Res. 88*, 1153–1172, 1983.

Emerman, S. H., and D. L. Turcotte, A fluid model for the shape of accetionary wedges, *Earth Planet. Sci. Lett., 63*, 379–384, 1983.

England, P. C., and T. J. B. Holland, Archimedes and the Tauren eclogites: The role of buoyancy in the preservation of exotic eclogite blocks, *Earth Planet. Sci. Lett., 44*, 287–294, 1979.

Fisher, M. A., R. von Huene, G. L. Smith, and T. R. Bruns, Possible seismic reflections from the downgoing Pacific plate, 275 kilometers from the eastern Aleutian trench, *J. Geophys. Res., 88*, 5835–5849, 1983.

Fix, J. E., The crust and upper mantle of central Mexico, *Geophys. J. R. Astron. Soc., 43*, 453–499, 1975.

Fryer, P., E. L. Ambos, and D. M. Hussong, Origin and emplacement of Mariana forearc seamounts, *Geology, 13*, 774–777, 1985.

Hasegawa, A., N. Umino, and A. Takagi, Double-planed structure of the deep seismic zone in the northeastern Japan arc, *Tectonophysics, 47*, 43–58, 1978.

House, L. S., and K. H. Jacob, Earthquakes, plate subduction, and stress reversals in the eastern Aleutian arc, *J. Geophys. Res., 88*, 9347–9373, 1983.

Hussong, D. M., and S. Uyeda, Tectonic processes and the history of the Mariana arc: A synthesis of the results of Deep Sea Drilling Project leg 60, *Initial Rep. Deep Sea Drill. Proj., 60*, 909–929, 1982.

Jackson, M. P. A., and C. J. Talbot, External shapes, strain rates, and dynamics of salt structures, *Geol. Soc. Am. Bull., 97*, 305–323, 1986.

Jischke, M. C., On the dynamics of descending lithospheric plates and slip zones, *J. Geophys. Res., 80*, 4809–4813, 1975.

Kanamori, H., The energy release in great earthquakes, *J. Geophys. Res., 82*, 2981–2987, 1977.

Karig, D. E., Evolution of arc systems in the western Pacific, *Annu. Rev. Earth Planet. Sci., 2*, 51–75, 1974.

Karig, D. E., and B. Ranken, Marine geology of the forearc region, southern Mariana Island arc, in *The Tectonic and Geologic Evolution of Southeast Asian Seas and Islands, Part 2, Geophys. Monogr. Ser.*, vol. 27, edited by D. E. Hayes, pp. 266–280, AGU, Washington, D. C., 1983.

Kehle, R. O., Analysis of gravity sliding and orogenic translation, *Geol. Soc. Am. Bull., 81* 1641–1664, 1970.

Lighthill, M. J., and G. B Whitham, On kinematic waves, I, Flood movement in long rivers, *Proc. R. Soc. London, Ser. A, 229*, 281–316, 1955*a*.

Lighthill, M. J., and G. B. Whitham, On kinematic waves, II, A theory of traffic flow on long crowded roads, *Proc. R. Soc. London, Ser. A, 229*, 317–345, 1955*b*.

Moore, J. C., Selective subduction, *Geology, 3*, 530–532, 1975.

Moore, J. C., J. S. Watkins, T. H. Shipley, K. J. McMillen, S. B. Bachman, and N. Lundberg, Geology and tectonic evolution of a juvenile accretionary terrane along a truncated convergent margin: Synthesis of results from leg 66 of the Deep Sea Drilling Project, southern Mexico, *Geol. Soc. Am. Bull., 93*, 847–861, 1982.

Pavlis, T. L., and R. L. Bruhn, Deep seated flow as a mechanism for the uplift of broad forearc ridges and its role in the exposure of high *P/T* metamorphic terranes, *Tectonics, 2*, 473–497, 1983.

Prager, W., *Introduction to Mechanics of Continua*, 230 pp., Ginn, Boston, Mass., 1961.

Ranken, B., R. K. Caldwell, and D. E. Karig, Kinematics of the Philippine Sea plate, *Tectonics, 3*, 555–575, 1984.

Reyners, R., and K. S. Coles, Fine structure of the dipping seismic zone and subduction mechanics in the Shumagin Islands, Alaska, *J. Geophys. Res., 87*, 356–366, 1982.

Sager, W. W., Mariana arc structure inferred from gravity and seismic data, *J. Geophys. Res., 85*, 5382–5388, 1980.

Samowitz, I. R., and D. W. Forsyth, Double seismic zone beneath the Mariana island arc, *J. Geophys. Res., 86*, 7013–7021, 1981.

Shor, G. G., Jr., and R. von Huene, Marine seismic refraction studies near Kodiak, Alaska, *Geophysics, 37*, 697–700, 1972.

Sorokhtin, O. G., and L. I. Lobkovskiy, The mechanism of subduction of oceanic sediments into a zone of underthrusting of lithospheric plates, *Izv. Acad Sci USSR Phys. Solid Earth*, Engl. Transl., *12*, 289–293, 1976.

Speed, R. C., and D. K. Larue, Barbados: Architecture and implications for accretion, *J. Geophys. Res., 87*, 3633–3643, 1982.

Stein, S., J. F. Engeln, and D. A. Wiens, Subduction seismicity and tectonics in the Lesser Antilles arc, *J. Geophys. Res., 87*, 8642–8664, 1982.

Stockmal, G. S., Modeling of large-scale accretionary wedge deformation, *J. Geophys. Res., 88*, 8271–8287, 1983.

Sugimura, A., and S. Uyeda, *Island Arcs: Japan and Its Environs*, 247 pp., Elsevier, New York, 1973.

Tharp, T. M., Numerical models of subduction and forearc deformation, *Geophys. J. R. Astron. Soc., 80*, 419–437, 1985.

von Huene, R., Structure of the outer convergent margin off Kodiak Island, Alaska, from multichannel seismic records, *Mem. Am. Assoc. Pet. Geol., 29*, 261–272, 1979.

von Huene, R., Tectonic processes along the front of modern convergent margins—research of the past decade, *Annu. Rev. Earth Planet. Sci., 12*, 359–381, 1984.

von Huene, R., G. W. Moore, and J. C. Moore, Cross section of Alaska Peninsula–Kodiak Island–Aleutian Trench, *Map and Chart Ser., MC-28A*, 3 pp., plus 2 map sheets, Geol. Soc. of Am., Boulder, Colo., 1979.

von Huene, R., M. Langseth, N. Nasu, and H. Okada, A summary of Cenozoic tectonic history along the IPOD Japan Trench transect, *Geol. Soc. Am. Bull., 93*, 829–846, 1982.

Watts, A. B., Gravity field of the northwest Pacific Ocean basin and its margin: Philippine Sea, *Map and Chart Ser., MC-12*, Geol. Soc. of Am., Boulder, Colo., 1976.

Westbrook, G. K., The structure of the crust and upper mantle in the region of Barbados and the Lesser Antilles, *Geophys. J. R. Astron. Soc., 43*, 201–242, 1975.

Westbrook, G. K., and M. J. Smith, Long décollements and mud volcanoes: Evidence from the Barbados ridge complex for the role of high pore-fluid pressure in the development of an accretionary complex, *Geology, 11*, 279–283, 1983.

M. Cloos, Department of Geological Sciences, University of Texas, Austin, TX 78713.

R. Shreve, Department of Earth and Space Sciences, University of California, Los Angeles, CA 90024.

(Received May 28, 1985;
revised April 21, 1986;
accepted May 16, 1986.)